ELSEVIER

Contents lists available at ScienceDirect

Gondwana Research

journal homepage: www.elsevier.com/locate/gr





Persistent Amazonian and West African detrital zircon signature in the northern Mauritanide Belt

Roberto Jiménez Borrego ^{a,*}, David Martínez Poyatos ^a, Antonio Azor ^a, Cristina Accotto ^a, Antonio Jabaloy-Sánchez ^a, Francisco González Lodeiro ^a, Mohamed Salem Sabar ^b, Ahmed Hamoud ^b, Ahmed Ould Ely Lekouyrie ^b

ARTICLE INFO

Keywords: Mauritanide Belt West African Craton Amazonian Craton Provenance study late Neoproterozoic rift

ABSTRACT

We provide new detrital zircon U/Pb geochronological data from nine samples of Neoproterozoic-Cambrian metasedimentary rocks of the northern Mauritanide Belt, aiming at constraining depositional ages and provenance in the paleotectonic context of the Rodinia to Gondwana supercontinent transition. The youngest detrital zircon populations indicate the following maximum depositional ages: c. 900 Ma (early Tonian) for the Atilis Quartzite Formation, c. 660 Ma (Cryogenian) for the gneissic Hajar Dekhen-Kleouat Unit, c. 580 Ma (middle Ediacaran) for the Atomai Formation, and c. 540 Ma (late Ediacaran-early Cambrian) for the Sainte Barbe Formation and the ophiolite-like Agoualilet Unit. Two types of zircon age distributions were identified, reflecting the most reliable original sources. Type I age spectra include c. 2.8 Ga, 2.1 Ga and 0.6 Ga age populations, which are interpreted to derive from West African Craton sources (Leonian/Liberian, Eburnean, Pan-African orogenies). Type I signature is found in the Atomai and Sainte Barbe formations and the Agoualilet Unit. Type II age spectra include, besides the type I populations, c. 1.8, 1.5, 1.2 and 1.0 Ga age populations, which are thought to derive from sources in the Amazonian Craton (Central Amazonian, Trans-Amazonian, Rio Negro-Juruena, Rondonian-San Ignacio, Sunsás-Grenvillian and Brasiliano orogenies). Type II signature is found in the Atilis Quartzite and Atomai formations, Hajar Dekhen-Kleouat Unit, and the Cambrian Nouatil Group (intra-WAC Taoudeni Basin). The changes in the detrital zircon record through the studied Neoproterozoic-Cambrian successions resulted from shifts in drainage systems and alternating sediment supply from both the West African and the Amazonian cratons along most of the Neoproterozoic period. Finally, we interpret that the subsequent opening of a shortlived oceanic realm (the Clymene Ocean) during the latest Ediacaran between the West African and the Amazonian cratons interrupted the direct sediment supply from the Amazonian Craton.

1. Introduction

Most of the various cratons that once formed the supercontinent Rodinia at approximately 1 Ga ago, were separated during early Neoproterozoic break-up (c. 900–800 Ma) and subsequently reassembled at late Neoproterozoic time (c. 600–550 Ma) to form a younger supercontinent, namely Gondwana (e.g., Cordani et al., 2003). The accretion of this supercontinent involved convergence/collision of, among others, the West African, Amazonian, São Francisco, and Parnaíba cratons (Fig. 1a), leading to the formation of various Neoproterozoic–early Paleozoic Brasiliano/Pan-African orogenic belts (e.g., Villeneuve and Cornée, 1994; Tohver et al., 2010; McGee et al., 2018; Villeneuve et al.,

2025). Among these cratons, the West African Craton (WAC) is primarily composed of an Archean–Paleoproterozoic basement, which crops out in the Leo-Man and Reguibat shields and underlies the intracratonic/pericratonic Taoudeni, Tindouf, Bove, and Volta basins (Fig. 1a) (Pitfield et al., 2004; Bradley et al., 2015). The western margin of the WAC (from Senegal to Morocco) is bordered by Neoproterozoic–early Paleozoic belts that were reworked during the late Paleozoic orogenic events (Bea et al., 2020; Villeneuve and Rossignol, 2023) and can thus attest several suture zones. One of these belts, the so-called Mauritanide Belt (Fig. 1b), which is the focus of this paper, features several tectonostratigraphic units separated by fault zones (Fig. 2), whose origin and paleogeographic significance remain uncertain (Martyn and Strickland, 2004;

^a Department of Geodynamics, University of Granada, Campus Fuentenueva, 18002, Spain

^b Département de Géologie, Faculté des Sciences et de la Technologie, Université de Nouakchott Al-Aasriya, BP 5026 Nouakchott, Mauritania

^{*} Corresponding author at: Department of Geodynamics, University of Granada, Campus Fuentenueva, 18002, Spain. *E-mail address:* robertojb@ugr.es (R.J. Borrego).

Pitfield et al., 2004; Bradley et al., 2015 and 2022).

The systematic geochronological study of detrital zircon grains in (meta)sedimentary rocks has significantly contributed to paleogeographic/paleotectonic reconstructions of pre-Permian orogens and supercontinents (e.g., Turner et al., 2014; Foster et al., 2015) by providing important information about the sources of the sediments. Furthermore, the availability of paleomagnetic data allows constraining such reconstructions (e.g., Pisarevsky et al., 2014). Nevertheless, the conclusions of these studies are far from unambiguous, because of the scarcity of paleomagnetic data, and the fact that some of the observed detrital zircon populations may have been recycled from intermediate sediment repositories (e.g., Pereira and Gama, 2021).

Regional compilations of igneous ages from the WAC (e.g., Grenholm et al., 2019) reveal a distinct late Paleoproterozoic–early Neoproterozoic magmatic gap (c. 1.9–0.9 Ga). On the other hand, detrital zircon geochronology results also do not reflect any major metamorphic or magmatic episode during the late Paleoproterozoic–early Neoproterozoic in the region (Kalsbeek et al., 2008; Nance et al., 2008; Bradley et al., 2015; Ait Lahna et al., 2020). However, some

Mesoproterozoic detrital zircon populations have been reported in sedimentary and metasedimentary rocks from belts and basins surrounding the WAC to the west, such as the Soutufide Belt (Bea et al., 2020), the Bove Basin (Villeneuve et al., 2025), and mainly the Mauritanide Belt and the western part of the Taoudeni Basin (Bradley et al., 2015 and 2022). The presence of Mesoproterozoic detrital zircons grains in the WAC sequences points to one or more exotic Mesoproterozoic sources after Rodinia breakup, being the Amazonian Craton the proposed source in many reconstructions (Keppie et al., 2003; Nance et al., 2008; Waldron et al., 2014; Bradley et al., 2022).

This study aims to unravel the paleogeographic evolution during the Neoproterozoic—early Cambrian of the northern Mauritanide Belt in the Akjoujt area. We report new detrital zircon U-Pb data from nine metasandstone samples from Neoproterozoic—early Cambrian successions in different tectonostratigraphic units of the Akjoujt area, and we discuss them in combination with published data (Bradley et al., 2022). Our results constrain the stratigraphic age of the rocks in this region and their provenance. On a broader context, a new model emerges that highlights the influence of an Ediacaran rift between the WAC and the

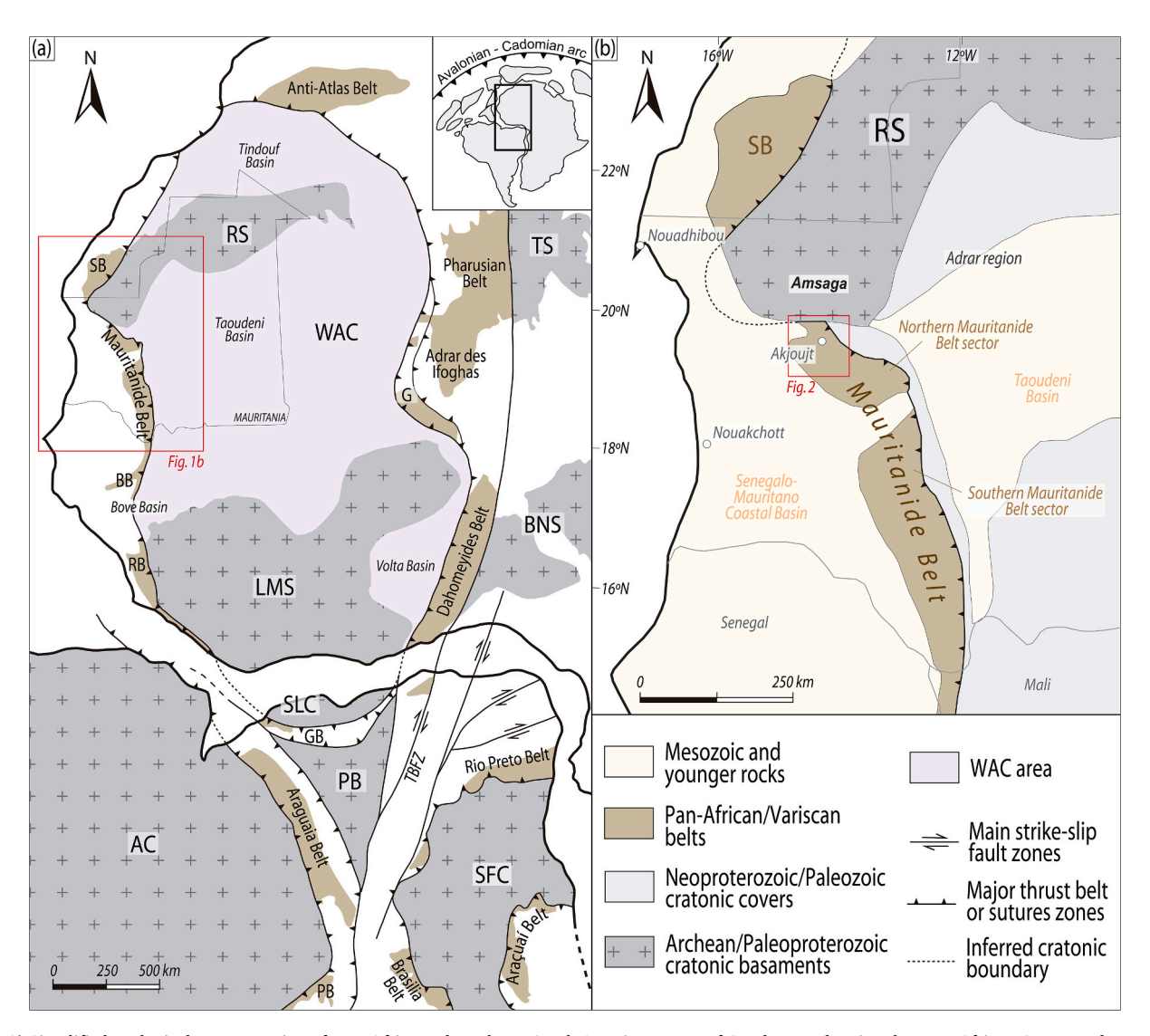


Fig. 1. A) Simplified geological reconstruction of west Africa and northeast South America as part of Gondwana, showing the West African Craton and surrounding belts (modified from Villeneuve and Rossignol, 2023). Cratons and shields: AC (Amazonian Craton), BNS (Benino-Nigerian Shield), LMS (Leo-Man Shield), PB (Parnaíba Block), RS (Reguibat Shield), SFC (São Francisco Craton), SLC (São Luis Craton), TS (Tuareg Shield) and WAC (West African Craton), partly covered by younger sedimentary cover). Belts: BB (Bassarides), GB (Gurupi Belt), PB (Paraguay Belt). RB (Rokelides Belt) and SB (Soutufide Belt). Rift: G (Gourma). Strike-slip fault zones: TBFZ (Transbrasiliano Fault Zone). The inset shows the large-scale late Neoproterozoic scenario with the study area located south of the Avalonian-Cadomian arc (simplified from Linnemann et al., 2008). b) Simplified geological map of western Mauritania (modified from Bradley et al., 2015).

Amazonian Craton, contributing to the paleotectonic reconstruction of the Rodinia-to-Gondwana transition.

2. Geological setting

The Mauritanide Belt (Fig. 1), located at the western margin of the WAC, is a poly-orogenic mountain belt likely resulting from the

superposition of Neoproterozoic (Pan-African) and late Paleozoic (Carboniferous) tectono-metamorphic events (e.g., Martyn and Strickland, 2004; Pitfield et al., 2004). The WAC is composed of a *meta*-igneous high-grade metamorphic basement, which crops out in the Reguibat Shield, to the north, and the Leo-Man Shield, to the south (Fig. 1a). The Reguibat Shield consists of gneissic and granitic rocks (Schofield et al., 2006; Pitfield et al., 2004; Key et al., 2008) and is

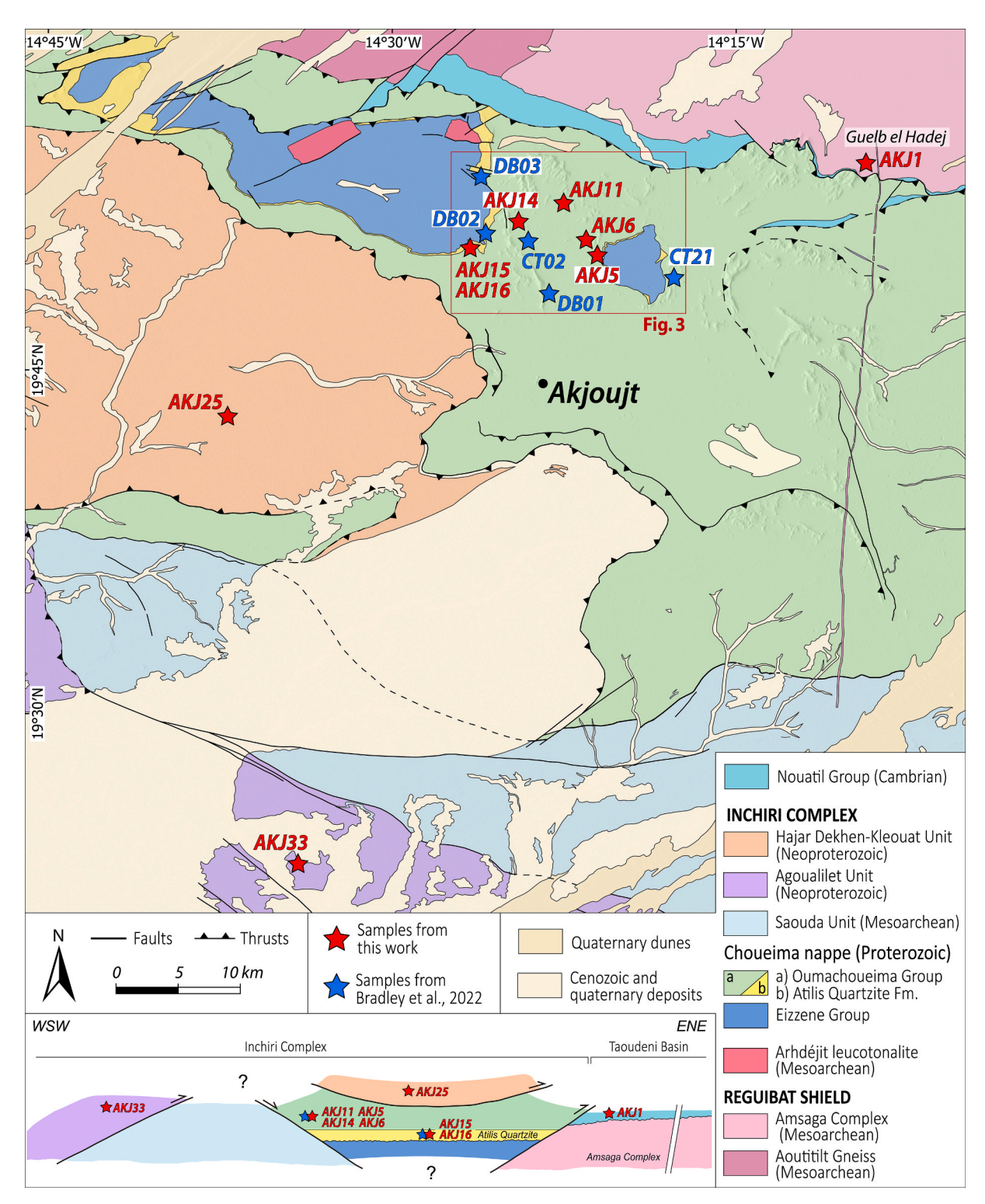


Fig. 2. Simplified geological map of the Akjoujt area (modified from Pitfield et al., 2004). Stars indicate the location of the samples studied in this work (in red) and samples already published (in blue; Bradley et al., 2022). The red square refers to the detailed geological map shown in Fig. 3. Lower inset: sketch of the inferred geometric relationships between the different tectonostratigraphic units of the Inchiri Complex, Nouatil Group and Amsaga Complex (not to scale).

subdivided into a southwestern province (namely Amsaga, northwestern Mauritania; Fig. 1b), where Archaean rocks predominate, and a northeastern province with Eburnean (c. 2.1 Ga) rocks (Rocci et al., 1991; Potrel et al., 1998; Schofield et al., 2006; Key et al., 2008). Large areas of the WAC are covered by subhorizontal sedimentary sequences, such as the one exposed in the large intracratonic Taoudeni Basin (Fig. 1b). It comprises Mesoproterozoic to Devonian sedimentary successions, dominated by siliciclastic rocks deposited in continental to shallow marine environments, and some coastal carbonate rocks (Pitfield et al., 2004, Bradley et al., 2022).

The Mauritanide Belt (Fig. 1b) extends for more than 1500 km, crossing the Mauritanian territory in a roughly north–south direction, and connecting to the north with the Soutufide Belt in the Western Sahara. To the west, the Mauritanide Belt is covered by the Meso–Cenozoic rift- and passive-margin sediments of the Senegalo-Mauritano Coastal Basin.

The tectonic architecture of the Mauritanide Belt includes an east-verging late Paleozoic (Variscan) frontal thrust (Lécorché and Clauer, 1984), which emplaces the entire belt onto the western border of the WAC basement and the Mesoproterozoic to Paleozoic sedimentary cover of the Taoudeni Basin. However, the main tectonothermal evolution of the belt is probably the result of superposed Pan-African (c. 800–500 Ma) (Dallmeyer and Lécorché, 1989), Caledonian (c. 490–390 Ma) (Bea et al., 2020) and Variscan (c. 390–300 Ma) (Le Goff et al., 2001) events. The Mauritanide Belt is subdivided into a southern sector with an approximately north–south structural grain, and a northern sector with northwest-southeast structural trends (Fig. 1b). The study area of this work (Akjoujt area; Fig. 1b and Fig. 2) is located in the northern sector of the Mauritanide Belt. The geological description given below follows the information available in geological maps (Pitfield et al., 2004; Bradley et al., 2015) and regional studies (Martyn and Strickland, 2004).

In the Akjoujt area, the northern Mauritanide Belt sector is relatively well exposed in a desertic low-relief region, where small outcrops appear isolated and surrounded by sand and gravel deposits. The main topographic ridges are marked by the numerous escarpments of banded iron formations (BIFs). The area is bounded to the northwest and southeast by large NE-SW trending active dune systems (Fig. 2).

2.1. The Amsaga Complex (WAC)

The Mesoarchaean crystalline basement, locally known as Amsaga Complex, crops out along the north-northeastern edge of the Akjoujt area (Fig. 1b and Fig. 2). It comprises the southwesternmost part of the Reguibat Shield, although it is thought to underlie the entire area, increasing in depth towards the southwest below the Mauritanide Belt (Martyn and Strickland, 2004). It consists of migmatitic gneisses, porphyritic granites variably deformed to augen-gneisses, amphibolite gneisses, coarse-grained tonalitic orthogneisses, schists and ironstones (Bradley et al., 2015). As part of the Amsaga Complex, a strongly foliated porphyritic orthogneiss crops out, namely the Aoutitilt Gneiss (Fig. 2), which was dated at 2954 \pm 11 Ma (Pitfield et al., 2004).

2.2. The Taoudeni Basin

The Mesoproterozoic–early Cambrian succession of the northern Taoudeni Basin exposed in Mauritania (known as the Adrar region, east of Akjoujt; Fig. 1b) is divided into five well-defined groups, separated by unconformities (Moussine-Pouchkine and Bertrand-Sarfati, 1997; Pitfield et al., 2004; Deynoux et al., 2006). From bottom to top, these groups are: (i) the Mesoproterozoic, mostly siliciclastic Char Group, which unconformably overlies the metamorphic basement (i.e., Amsaga Complex, Reguibat Shield), covered by (ii) the late Mesoproterozoic–early Neoproterozoic carbonate-rich Atar Group, which, in turn, is overlain by (iii) the Neoproterozoic mostly siliciclastic Assabet el Hassiane Group. The Char, Atar and Assabet el Hassiane groups are unconformably overlain by (iv) the tillites of the Jbeliat Group, attributed

to the Neoproterozoic (Marinoan glaciation; Pitfield et al., 2004; Deynoux et al., 2006; Bradley et al., 2022) or to the early Cambrian (Moussine-Pouchkine and Bertrand-Sarfati, 1997; Albert-Villanueva et al., 2016). Finally, up section there are (v) the carbonate and siliciclastic rocks of the Teniagouri Group, assigned to the Neoproterozoic (Pitfield et al., 2004; Deynoux et al., 2006; Bradley et al., 2022) or to the early Cambrian (Moussine-Pouchkine and Bertrand-Sarfati, 1997; Albert-Villanueva et al., 2016).

The Nouatil Group unconformably overlies (Pitfield et al., 2004) the above-mentioned stratigraphic succession in the Adrar region. It comprises c. 500 m of an early Cambrian siliciclastic succession, made up of fine red sandstones and siltstones with a basal conglomerate, and subordinate dolostones and limestones, deposited in a shallow marine to fluvial environment (Pitfield et al., 2004). In the Akjoujt area (Fig. 2), this group crops out along a northwest-southeast trending band situated between the northern edge of the Mauritanide Belt (Inchiri Complex) and the Amsaga Complex (southwestern edge of the Reguibat Shield). In this region, the Nouatil Group unconformably overlies the Amsaga Complex and is, in turn, overthrust by the (meta)volcano-sedimentary sequence of the Choueima nappe (Variscan frontal thrust; Fig. 2).

2.3. The North Mauritanide sector (Inchiri Complex)

The Inchiri Complex, named after the eponymous region in western Mauritania, whose capital is Akjoujt, comprises a set of tectonic units, which, from southwest to northeast, are as follows: Agoualilet Unit, Saouda Unit, Hajar Dekhen-Kleouat Unit and the Choueima nappe (Fig. 2). These units record at least one penetrative deformation, which gave way to a low-dipping main foliation. At outcrop scale, the main foliation is related to asymmetric folds that do not develop large-scale reversed limbs. In some cases (e.g., the Hajar Dekhen-Kleouat Unit), the main foliation is mylonitic and likely related to ductile simple shearing. Later deformations include open upright folds, which, together with late brittle faults, are responsible for the cartographic pattern. The inferred geometrical relationships between the different units are shown at the lower inset of Fig. 2.

2.3.1. The Agoualilet Unit

The Agoualilet Unit is poorly exposed along a northwest-southeast trending strip, which seems to overlie the Saouda Unit located to the north. It is composed of a mélange of mafic rocks including metaultramafites, metagabbros, metabasalts, amphibolites, and as well as quartzites, sandstones, and psammitic to semipelitic schists, with scattered lenses of metaconglomerates, metacherts and BIFs (Pitfield et al., 2004). This unit has been interpreted as a possible ophibilitic sequence, loosely attributed to the Proterozoic (Pitfield et al., 2004; Bradley et al., 2015).

2.3.2. The Saouda Unit

The Saouda Unit is composed of a deformed sequence of schists, amphibolites, orthogneisses, metaquartzites, and both felsic and mafic metavolcanic rocks, with alternating BIFs and ferruginous quartzites (Pitfield et al., 2004). This unit is attributed to the Mesoarchean and, hence, virtually coeval with the Amsaga Complex (Marcelin, 1968, Pitfield et al., 2004). The Saouda Unit poorly crops out along a broadly east—west trending band located south of the Choueima nappe and the Hajar Dekhen-Kleouat Unit, being separated from them by a north-dipping normal fault (Fig. 2).

2.3.3. The Hajar Dekhen-Kleouat Unit

The Hajar Dekhen-Kleouat Unit is exposed west and south of Akjoujt (Fig. 2). It comprises an association of Neoproterozoic rocks (*augen*-gneisses and metagranitic rocks with minor amphibolites, intercalated with scarce quartzites, psammitic schists, and marbles), affected by ductile (mylonitic) deformation at amphibolite-facies metamorphic conditions (Pitfield et al., 2004). The unit depicts an unrooted geometry

with upright open folds and a basal thrust onto the Choueima nappe.

2.3.4. The Choueima nappe

This is the most widely exposed unit of the Inchiri Complex in the Akjoujt area (Fig. 2) and consists of a tectonically imbricated sequence of metasedimentary and metavolcanic rocks, ascribed to the Neoproterozoic, and deformed at low-grade metamorphic conditions. The sequence is divided into a lower succession, known as the Eizzene Group, which comprises two formations (Pitfield et al., 2004): the lower Raoui Formation, consisting of fine-grained altered metabasalts, overlain by the entirely metasedimentary Khmeiyat Formation composed of schists and phyllites, with alternating thin bands of quartzite and metagreywackes, and BIFs (Fig. 3). In the largest outcrop of the Eizzene Group (northwest of Akjoujt; Fig. 2), two patches of fine- to mediumgrained biotite-bearing leucotonalite, known as the Arhdéjit Leucotonalite, are exposed. Their Mesoarchean age (2909 \pm 20 Ma, Pitfield et al., 2004) points to an old basement (equivalent to the Amsaga Complex), instead of intrusive granitoids in the Eizzene Group (Martyn and Strickland, 2004).

The Oumachoueima Group unconformably overlies the Eizzene Group (Fig. 2 and Fig. 3) and has been stratigraphically divided into a series of formations (Martyn and Strickland, 2004; Pitfield et al., 2004). The lowermost formation is orthoquartzitic, namely the Atilis Quartzite Formation, with a thickness ranging from a few tens of meters up to 500 m. The Atilis Quartzite Formation truncates the BIF units of the Eizzene Group and clearly delineates an unconformity at the base of the Oumachoueima Group (Martyn and Strickland, 2004; Pitfield et al., 2004). The Irarchene el Hamra Formation is exposed above the Atilis Quartzite Formation and is made up of quartz-rich metagreywackes,

metalimonites and metavolcanoclastic rocks. Overlying the Irarchene el Hamra Formation, the Atomai and Sainte Barbe formations crop out, composed of predominant mafic metavolcanoclastic rocks at the base, which evolve upwards to metandesites and metarhyodacites. Finally, the Akjoujt Formation is composed of submarine tholeitic metabasalts and microgabbros (Pitfield et al., 2004; Bradley et al., 2015). Discontinuous BIF horizons appear at several stratigraphic levels within the Eizzene and Oumachoueima groups. The most important BIF is the so-called Lembeitih Formation, located at the contact between the Sainte Barbe Formation and the Akjoujt Formation, with an approximate thickness of 20 m and good exposure throughout the entire Akjoujt area, thus serving as a remarkable cartographic and stratigraphic marker. Another prominent BIF horizon is located on top of the Atomai Formation (Fig. 3).

3. Samples and methods

Approximately 4 kg per each of the nine studied samples were collected from eight outcrops in the Akjoujt region (Fig. 2). The location of the nine samples and other details are synthetized in Table 1. Sample AKJ1 was collected from a subhorizontal siliciclastic sedimentary level of the Nouatil Group (Taoudeni basin) cropping out at the hillslope of the Guelb el Hadej site, 31 km northeast of Akjoujt (Fig. 2). This sample is a quartz-feldspar sandstone, composed of rounded quartz grains and, to a lesser extent, feldspar and siderite grains, ranging from fine to medium grain size (c. 1–0.2 mm in diameter). Except for sample AKJ1, all the other samples correspond to variably deformed/recrystallized metasandstones from different units of the Inchiri Complex (Mauritanide Belt).

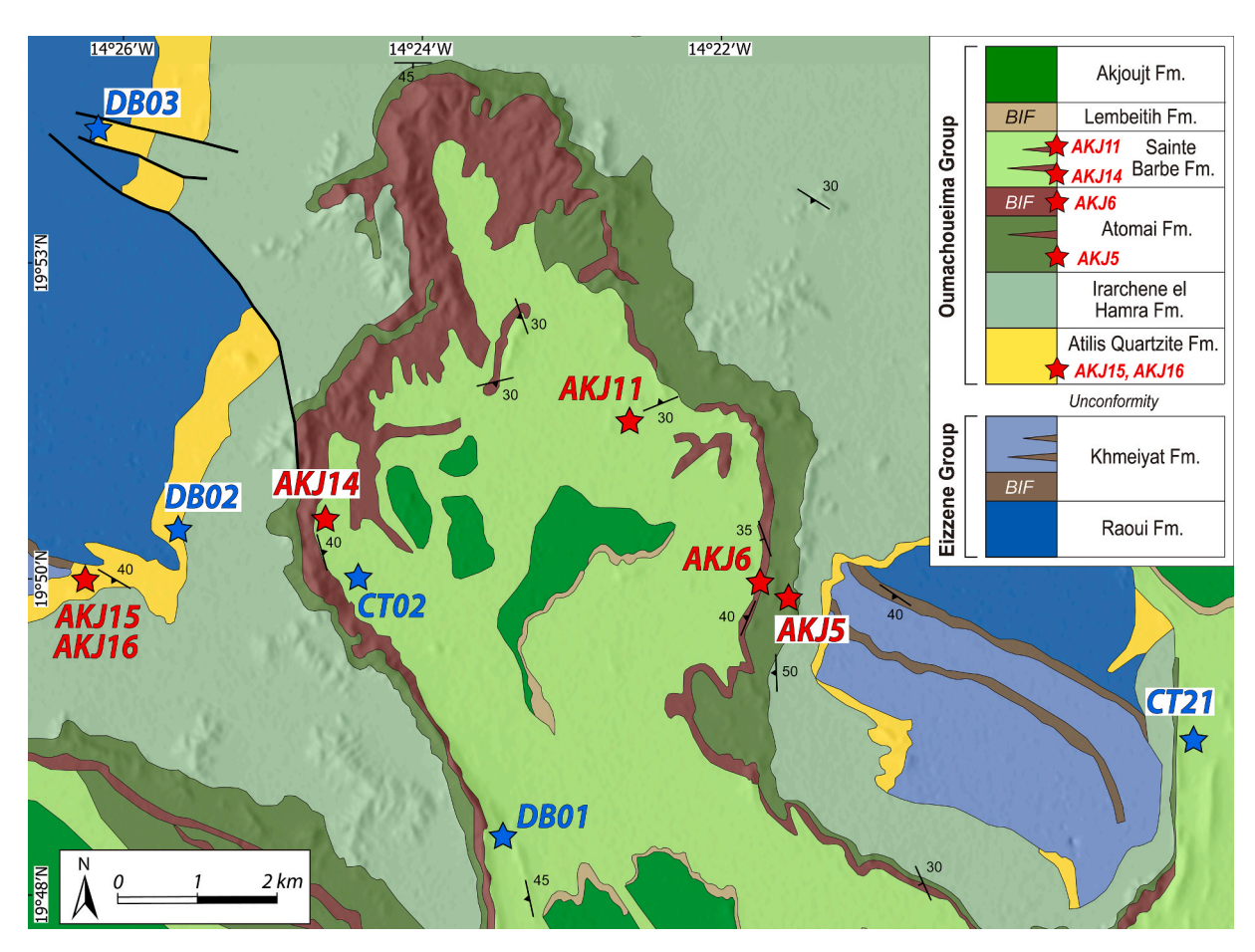


Fig.3. Detailed geological map of the northern Akjoujt area, including measurements of bedding and foliation (Pitfield et al., 2004; and own data). Stars indicate the location of the studied samples (in red) and other samples already published (in blue; from Bradley et al., 2022). Upper right inset is a schematic stratigraphic sequence (not to scale) of the Oumachoueima and Eizzene groups. Stars indicate the approximate location of the studied samples (in red).

Table 1
List and details of the samples studied. (*) total number of analyses performed vs concordant results (in bold).

	Location (UTM, WGS84)						U-Pb geochronology
Sample	Zone	X (East)	Y (North)	Unit/formation	Lithology	Stratigraphic age (according to Bradley et al., 2015 and 2022)	Analyses (*)
AKJ1	28N	588464	2200747	Taoudeni Basin, Nouatil Group	Quartz-feldspar sandstone	Early Cambrian	140/124
AKJ5	28N	568490	2193624	Oumachoueima Group, lower Atomai Formation	Quartzite	Late Neoproterozoic	60/ 45
AKJ6	28N	567958	2193782	Oumachoueima Group, upper Atomai Formation	Quartzitic sandstone	Late Neoproterozoic	140/117
AKJ11	28N	565765	2196433	Oumachoueima Group, upper Sainte Barbe Formation	Quartzite	Late Neoproterozoic-early Cambrian	140/ 109
AKJ14	28N	561371	2194821	Oumachoueima Gr, lower Sainte Barbe Formation	Quartzitic sandstone	Late Neoproterozoic-early Cambrian	50/31
AKJ15	28N	558095	2193975	Oumachoueima Group, Atilis Quartzite Formation	Quartzite	Early Neoproterozoic (Tonian)	140/139
AKJ16	28N	558095	2193975	Oumachoueima Group, Atilis Quartzite Formation	Quartzite	Early Neoproterozoic (Tonian)	140/ 140
AKJ25 AKJ33	28N 28N	540047 545397	2180399 2143868	Hajar Dekhen-Kleouat Unit Agoualilet Unit	Quartzite Quartzite	Neoproterozoic Neoproterozoic	140/ 107 140/ 116

Samples AKJ5, AKJ6, AKJ11, AKJ14, AKJ15 and AKJ16 were collected from different outcrops of the low-grade metasedimentary and metavolcanic succession of the Oumachoueima Group, in an area located 10-15 km north of Akjoujt (Fig. 3). Samples AKJ15 and AKJ16 were collected from an outcrop of the Atilis Quartzite Formation (lower formation of the Oumachoueima Group). Sample AKJ15 is a quartzite consisting of fine- to medium-sized quartz grains (c. 0.1-0.2 mm in diameter) embedded in a microcrystalline quartz matrix, with subordinate interstitial phyllosilicates and/or iron oxides. Sample AKJ16 is a quartzite composed of fine-sized quartz grains (c. 0.1 mm in diameter) elongated parallel to a weak foliation, with siderite, iron ores, and subordinate phyllosilicates, all embedded in a microcrystalline quartz matrix. Sample AKJ5 comes from the lower Atomai Formation and is a metasandstone mainly consisting of medium-sized quartz grains (c. 0.2 mm in diameter), which appear slightly elongated parallel to a weak foliation and embedded in a matrix of microcrystalline quartz, phyllosilicates, and subordinate iron oxides. Sample AKJ6 corresponds to the BIF horizon located on top of the Atomai Formation and is a quartzitic metasandstone mainly composed of fine-sized quartz grains (c. 0.1 mm), highly remobilized and replaced by iron ores defining a compositional banding. Sample AKJ14, from the lower Sainte Barbe Formation, is a metasandstone composed of very fine-sized quartz grains (< 0.1 mm in diameter) with abundant phyllosilicates and iron ores. Sample AKJ11 was collected from the upper Sainte Barbe Formation, and is a quartzite composed of very fine- to fine-sized quartz grains (c. 0.05-0.1 mm in diameter).

Sample AKJ25 was collected from a quartzite intercalation in the gneissic Hajar Dekhen-Kleouat Unit, 25 km west of Akjoujt (Fig. 2); it is made up of fine-sized quartz grains (c. 0.1 mm in diameter). Finally, sample AKJ33 was collected 25 km southwest of Akjoujt, in the ophiolitic-like Agoualilet Unit (Fig. 2), and is a quartzite with fine- to coarse-sized quartz grains (c. 0.1-0.3 mm in diameter).

All samples were processed in the laboratories of the Department of Geodynamics at the University of Granada (Spain). The samples were crushed using a jaw crusher and mineral grains were separated using granulometric (sieving), density (panning) and magnetic procedures, resulting in a heavy mineral concentrate. The concentrate was sent to the John de Laeter Centre at Curtin University in Perth (Australia), where, whenever possible, 150 to 200 zircon grains were handpicked from each sample. Once the zircons were selected, mounted in epoxy and cut to half-height, cathodoluminescence images (Fig. 4) were taken using the MIRA3 TESCAN instrument at the Microscopy and Microanalysis Facility. After visual inspection and spot selection, zircons were analyzed for U, Th and Pb isotopes with laser ablation inductively

coupled plasma mass spectrometry (LA-ICPMS). Individual zircon grains were ablated using a RESOlution 193 nm excimer laser, with 24 μ m beam and laser energy of 2 J/m2, for 25 s at 6 Hz laser repetition rate.

To obtain a statistically significant amount of data (Vermeesch, 2004), 140 analyses were performed on each sample whenever possible, and results with discordance greater than 10 % were excluded from further processing (Spencer et al., 2016). Due to the increasing errors associated with ²⁰⁶Pb/²³⁸U data on old grains, ages were calculated with this isotopic ratio only for zircon grains younger than 1.5 Ga, while 207 Pb/ 206 Pb results were used for older grains (Spencer et al., 2016). For all analyses, the following (primary or secondary) reference materials were used: OGC (3465.4 \pm 0.6 Ma; Stern et al., 2009), 91,500 (1063.78 \pm 0.65 Ma; Wiedenbeck et al., 1995), GJ1 (608.53 \pm 0.37 Ma; Jackson et al., 2004), Plešovice (337.13 ± 0.37 Ma; Sláma et al., 2008), Maniitsoq (3008.70 \pm 0.72 Ma; Marsh et al., 2019) and Rak-17 (295.56 \pm 0.21 Ma; G-chron standard, website of the International Association of Geoanalysts), with errors at the 2σ level. For zircons with $^{207}Pb/^{206}Pb$ ages > 1.5 Ga, the primary reference standard used was OG1, whereas for zircon grains < 1.5 Ga, the primary reference was 91500.

The statistical analysis of the data was conducted using the DensityPlotter 8.4 software (Vermeesch, 2012). Histograms were generated using 40 Ma intervals, and an adaptive bandwidth of 40 Ma was employed for Kernel Density Estimators (KDE). The average ages of the detrital zircon populations were determined using the mixturemodelling feature of DensityPlotter 8.4. All errors are presented at 1σ level. The maximum depositional age (MDA) of the samples in this study was estimated using the minimum age model referred to by Vermeesch (2021) as the Maximum Likelihood Age (MLA), through data visualization in radial plots via IsoplotR. This method has been demonstrated to be less susceptible to produce anomalously younger ages than other methods commonly applied (e.g., the youngest single grain, the youngest grain cluster at 1σ or 2σ , the weighted mean of the youngest three or four zircon dates; Coutts et al., 2019; Vermeesch, 2021). However, like other methods, it is not immune to errors induced by Pb loss. The MLA method converges towards the best solution by using the youngest detrital zircon population to generate a binary solution: a discrete minimum age peak (the MLA) and a log-normal distribution with the remaining young grains, truncated at the discrete minimum age peak. This approach accounts for unequal uncertainties in the data through the application of maximum likelihood estimation statistics (Vermeesch, 2021). It is important to note that the MLA coincides with the youngest single grain model when the young tail of a detrital age spectra is sparsely sampled and the age difference between the youngest and the second youngest grains is significantly greater than their respective



Fig. 4. Cathodoluminescence images of selected detrital zircon grains from the samples in this study. Each zircon grain shows the spot location and the result of the corresponding U-Pb analysis.

analytical uncertainties, as is the case for sample AKJ14 in this study. For MLA calculations, the IsoplotR software was employed, using a logarithmic transformation, namely the finite mixtures setting, adjusted to "minimum", and the 3-parameter model, in accordance with Vermeesch (2021).

4. Results

A synthesis of the total number of U-Pb analyses performed and the concordant results for each sample are presented in Table 1 (the detailed analytical dataset from LA-ICPMS is provided in the supplementary material as Supplementary Data S1). All the zircon grains analyzed in the nine studied samples range from 50 to 200 μ m. Most of them are grayish-whitish and yellowish in color, with shapes varying from rounded to sub-euhedral (Fig. 4).

In sample AKJ1 (Fig. 5a), 140 analyses were performed on 140 detrital zircon grains, yielding 124 concordant results. The main population in this sample accounts for 31.5 % of the data (n = 39), which define a Ectasian–Stenian peak (mean age of 1212 ± 1.2 Ma; interval of c. 1328-1079 Ma). A second-order population is Calymmian–Ectasian (mean age of 1443.6 ± 1.9 Ma; interval of c. 1586-1340 Ma; 25.8 % of the data; n = 32), while another two clusters yielded Orosirian–Statherian and Rhyacian–Orosirian mean ages (1758.8 ± 5.2 Ma, c. 1831-1643 Ma, 10.5 %, n = 13, and 1997.3 ± 3.9 Ma, c. 2106-1859 Ma, 12.1 %, n = 15). Two minor populations of Mesoarchean (2951.4 ± 3.8 Ma; c. 2979-2910 Ma; 4.8 %; n = 6) and Ediacaran (622.4 ± 1.7 Ma; c. 634-607 Ma; 4.8 %; n = 6) ages are also observed. Scattered data provided Stenian–Tonian ages (n = 5, c. 1040-945 Ma), Neoarchean–Rhyacian (n = 6, c. 2741-2158 Ma), and Paleoarchean ages (n = 2, c. 3348-3188 Ma). The dates yielded an Ediacaran MLA of 613.1 ± 4.8 Ma.

From sample AKJ5 (Fig. 5b), 60 zircon grains were analyzed, yielding 58 results, 45 of which were concordant. A total of 37.8 % of the data (n = 17) fall within a main population of Cryogenian–Ediacaran age (with a peak at 621.1 \pm 1.1 Ma; interval of c. 691–580 Ma). A subordinate population defines a Mesoarchean age (2948.1 \pm 2 Ma; c. 2970–2877 Ma; 28.9 %; n = 13). A minor Rhyacian–Orosirian population is also observed (peak at 2027.9 \pm 6.3 Ma, c. 2058–1936 Ma, 13.3 %, n = 6). Scattered analyses provided Orosirian–Tonian (n = 8, c. 1866–836 Ma), and Neoarchean ages (n = 1, c. 2693 Ma). The dates gave an Ediacaran MLA of 586.5 \pm 6.2 Ma.

A total of 140 detrital zircon grains were analyzed from sample AKJ6 (Fig. 5c), yielding 140 dates with 117 concordant results. The main population is Ectasian–Stenian (1242.1 \pm 1.2 Ma; c. 1374–1131 Ma; 31.6 %; n = 37). Five additional populations can be defined, with the following ages: Cryogenian–Ediacaran (612.4 \pm 1.1 Ma; c. 647–587 Ma; 12.8 %; n = 15), Stenian–Tonian (1028.6 \pm 2.3 Ma; c. 1074–987 Ma; 7.7 %; n = 9), Calymmian (1473.2 \pm 2.8 Ma; c. 1584–1415 Ma; 15.4 %; n = 18), Rhyacian–Statherian (1923 \pm 3.1 Ma; c. 2141–1717 Ma; 18.8 %; n = 22), and Mesoarchean (2971.6 \pm 2.8 Ma; c. 3038–2911 Ma; 8.5 %; n = 10). Scattered data provided Tonian (n = 1, c. 731 Ma), Neoarchean–Rhyacian (n = 4, c. 2755–2240 Ma), and early Mesoarchean ages (n = 1, c. 3164 Ma). An Ediacaran MLA of 595.6 \pm 5.6 Ma is derived from the dates.

From sample AKJ11 (Fig. 5d), 140 analyses were performed on 140 zircon grains, with 109 concordant results. The main population is Tonian–Ediacaran in age (634.7 \pm 0.6 Ma; c. 780–553 Ma; 58.7 %; n = 64). A second-order peak defines a Rhyacian–Orosirian population (2062.8 \pm 2.5 Ma; c. 2260–1967 Ma; 22.9 %; n = 25). Three minor populations of Stenian–Tonian (979.6 \pm 2.6 Ma; c. 1032–888 Ma; 5.5 %; n = 6), Ectasian–Stenian (1214.5 \pm 3.2 Ma; c. 1237–1161 Ma; 4.6 %; n = 5) and Orosirian–Statherian (1828 \pm 8.8 Ma; c. 1849–1789 Ma; 3.7 %; n = 4) ages are also observed. Scattered data provide Calymmian (n = 2; c. 1499–1405 Ma) and Mesoarchean–Neoarchean ages (n = 3; c. 2953–2508 Ma). The dates indicate an Ediacaran MLA (554.1 \pm 7.4 Ma).

In sample AKJ14 (Fig. 5e), 50 zircon grains were analyzed, yielding 49 results, 31 of which were concordant. Most of the data (41.9 %; n = 13) range from c. 644 to 552 Ma and define a Cryogenian–Ediacaran population with a mean age of 611 \pm 0.6 Ma. Minor Stenian–Tonian (980.1 \pm 2 Ma; c. 1031–943 Ma; 9.7 %; n = 3) and Rhyacian–Orosirian (2079.1 \pm 4.7 Ma; c. 2162–1955 Ma; 16.1 %; n = 5) populations are also observed. Scattered analyses yielded Orosirian–Ectasian (n = 4, c. 1244–1846 Ma) and Mesoarchean–Siderian (n = 6, c. 3190–2303 Ma) ages. The dates provide an Ediacaran MLA of 551.9 \pm 9.7 Ma.

A total of 140 detrital zircon grains were analyzed from sample AKJ15 (Fig. 5f), yielding 140 dates, of which 139 were concordant. The main population has a Ectasian–Stenian mean age (1239.5 \pm 1.2 Ma; c. 1390–1138 Ma; 46 %; n = 64). Additionally, five minor populations can be defined, with the following ages: Stenian–Tonian (997.3 \pm 1.6 Ma; c. 1073–885 Ma; 18 %; n = 25), Statherian–Calymmian (1497.9 \pm 2.7 Ma; c. 1609–1401 Ma; 15.8 %; n = 22), Orosirian–Statherian (1744.2 \pm 4.7 Ma; c. 1851–1693 Ma; 7.9 %; n = 11), Orosirian (1974.8 \pm 5.1 Ma, c. 2012–1926 Ma; 5.8 %; n = 8), and Mesoarchean–Neoarchean (2782.1 \pm 3.4 Ma; c. 2895–2702 Ma; 4.3 %; n = 6). Scattered data yielded Rhyacian ages (n = 3, c. 2168–2090 Ma). The dates gave a Tonian MLA of 896 \pm 17 Ma.

From the AKJ16 sample (Fig. 5g), 140 analyses were performed on 140 detrital zircon grains, all of them yielding concordant data. The main population in this sample depicts an Ectasian–Stenian peak centered at c. 1215.3 \pm 0.8 Ma (c. 1280–1139 Ma; 38.6 %; n = 54). A subordinate population also yielded a Statherian–Ectasian age (1412.1 \pm 1.6 Ma; c. 1617–1314 Ma; 30.7 %; n = 43). Minor populations gave Stenian–Tonian (1015.4 \pm 1.5 Ma; c. 1082–903 Ma; 11.4 %; n = 16) and Orosirian–Statherian (1888.7 \pm 4.1 Ma; c. 2029–1701 Ma; 15.7 %; n = 22) ages. Several scattered data indicated Cryogenian (n = 1, c. 707 Ma) and Mesoarchean–Rhyacian (n = 4, c. 2847–2091 Ma) ages. A Tonian MLA of 926 \pm 20 Ma is derived from the dates.

In sample AKJ25 (Fig. 5h), 140 analyses were performed on 140 zircon grains, yielding 107 concordant data. The two main populations showed Ectasian–Stenian and Stenian–Tonian ages, peaked at 1228.7 \pm 1.4 Ma (c. 1329–1163 Ma; 39.3 %; n = 42) and 1020 \pm 1.4 Ma (c. 1140–865 Ma; 32.7 %; n = 35) respectively. Furthermore, minor Tonian (772.5 \pm 2.4 Ma; c. 829–725 Ma; 7.5 %; n = 8), Calymmian–Ectasian (1431.3 \pm 3.5 Ma; c. 1470–1399 Ma; 10.3 %; n = 11) and Rhyacian–Orosirian (2076.6 \pm 9.2 Ma; c. 2101–2029 Ma; 4.7 %; n = 5) populations are also present. Scattered data provided Cryogenian (n = 1, c. 657 Ma), Orosirian–Calymmian (n = 4, c. 1871–1555 Ma), and Siderian (n = 1, c. 2444 Ma) ages. The dates provide a Cryogenian MLA of 662 \pm 14 Ma.

From sample AKJ33 (Fig. 5i), 140 grains were analyzed, yielding 140 results, 116 of which were concordant. The main population has a Cryogenian–Ediacaran age (614.5 \pm 0.6 Ma; c. 678–545 Ma; 48.3 %; n = 56). Rhyacian–Orosirian ages represent a second-order population (2017.8 \pm 2.7 Ma; c. 2111–1820 Ma; 22.4 %; n = 26). Additionally, two minor clusters of data define a Tonian–Cryogenian (791.2 \pm 1.8 Ma; c. 863–704 Ma; 9.5 %; n = 11), and a Stenian–Tonian (1049.6 \pm 2.5 Ma; c. 1141–990 Ma; 6 %; n = 7) populations. Scattered data gave Calymmian–Ectasian (c. 1540–1244 Ma; n = 3) and Mesoarchean–Rhyacian (c. 3027–2172 Ma; n = 13) ages. The dates yielded an Ediacaran MLA of 549 \pm 13 Ma.

5. Discussion

5.1. Maximum and True depositional ages

The youngest detrital zircon grains/populations in (meta)sedimentary rocks have become widely utilized to constrain their Maximum Depositional Age (MDA) (Sharman and Malkowski, 2020). This approach might serve as a proxy for True Depositional Ages (TDA), which are typically derived from geochronological dating of interbedded volcanic rocks and/or from biostratigraphy. If volcanic activity

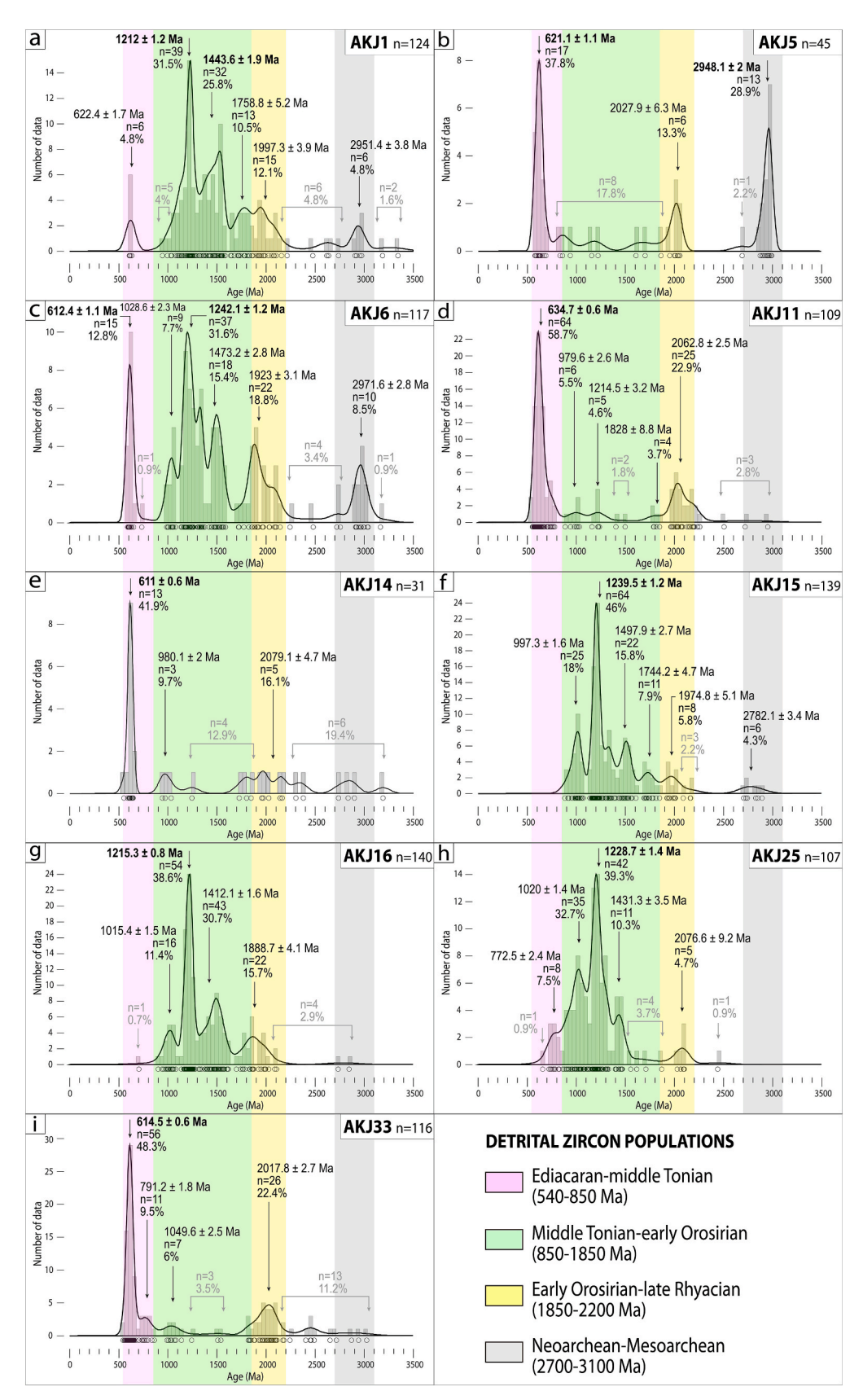


Fig. 5. U-Pb results. KDE (kernel density estimator; black lines) and histogram (gray bars) plots display the detrital zircon U-Pb geochronological results for each sample (a–i). The mean ages of the main populations for each sample are indicated in bold. The plots use 206 Pb/ 238 U ages for dates < 1500 Ma and 207 Pb/ 206 Pb ages for dates > 1500 Ma, with errors expressed at the 1σ level. Both KDE and histograms were created using DensityPlotter 8.4 (Vermeesch, 2012).

providing detrital zircon grains is coeval to sedimentation, MDAs may occasionally be coeval with (or close to) TDAs. However, MDAs are commonly older than TDAs. This discrepancy between MDAs and TDAs depends primarily on the geological and geographic context of sedimentation (e.g., Sharman and Malkowski, 2020). In this study, MDAs have been determined using the Maximum Likelihood Age (MLA) model (Vermeesch, 2021).

In the Akjouit area, TDAs are poorly constrained due to the absence of both fossil content and geochronological data from volcanic rocks intercalated within the sedimentary sequences (Pitfield et al., 2004). Therefore, MDAs may be used to discuss and partially constrain the TDAs of the metasedimentary rocks. Previous studies (Pitfield et al., 2004; Bradley et al., 2015) have attributed tentative Neoproterozoic stratigraphic ages to the Agoualilet and Hajar Dekhen-Kleouat units, and Tonian-early Cambrian ages to the Oumachoueima Group. The MDAs that emerged from our detrital zircon geochronological study agree with the proposed ages of these groups and refine them into the Neoproterozoic and early Cambrian. Nevertheless, a first step to ensure the validity of MDAs is to discard concealed (putative) Pb loss in the analyses related to post-magmatic processes, which could have rejuvenated the ages estimated (see for instance, Andersen et al., 2019). This has been done by projecting the raw analytical data on the Wetherill diagram (Supplementary Data S2). Most of the samples do not show any discordia lines due to Pb loss. In the few samples in which putative discordia lines could be traced, these correspond to analyses with discordance > 10 % and attributable to recent Pb loss (Andersen et al., 2019). In all cases, none of these putative Pb loss arrays could have affected the estimated MLAs, which plot right on the concordia line. Therefore, the MLAs and MDAs calculated in this work are considered to represent geologically valuable ages.

MDA of metasedimentary rocks of the ophiolitic-like Agoualilet Unit is late Ediacaran (c. 549 Ma, sample AKJ33, Fig. 6a). This age suggests that an oceanic realm might have developed during the latest Neoproterozoic between the WAC and the Amazonian Craton. The sample studied from the Hajar Dekhen-Kleouat Unit (AKJ25, Fig. 6a) yielded a Cryogenian MLA of c. 662 Ma. Furthermore, the TDA of the sedimentary rocks of the Hajar Dekhen-Kleouat Unit can be constrained from the numerous intrusive mostly felsic orthogneisses, where a protholith age of c. 599 Ma (U-Pb on zircon; Pitfield et al., 2004) was obtained. Therefore, the TDA of the Hajar Dekhen-Kleouat Unit is bracketed between c. 662 and 599 Ma (late Cryogenian–early Ediacaran). In addition, sample AKJ25 lacks the characteristic Ediacaran peak that is present in younger rocks from the region (see below), thus pointing to a late Cryogenian age for the Hajar Dekhen-Kleouat sedimentary rocks.

The samples from the Oumachoueima Group show MDAs from early Tonian to early Cambrian (Fig. 6a, b). On the one hand, the four samples from the Atilis Quartzite Formation, two from this study (samples AKJ15 and AKJ16) and two from Bradley et al. (2022) (Samples DB02 and DB03), yielded early Tonian MDAs (c. 896 to 984 Ma; Fig. 6b). On the other hand, the seven samples from the overlying Atomai and Sainte Barbe formations (samples AKJ5, AKJ6, AKJ14, and AKJ11 from this study; samples DB01, CT21, and CT02 from Bradley et al. (2022); Fig. 6b) yielded MDAs in the range middle Ediacaran-early Cambrian (c. 596-534 Ma), and all of them include a characteristic Ediacaran peak (see section 5.2.1.). According to the stratigraphic parallelism between all of these formations and the absence of putative erosive levels, an apparently continuous sedimentation would be inferred for the whole Oumachoueima Group (Martyn and Strickland, 2004; Pitfield et al., 2004). In this regard and considering the youngest zircon grain (c. 593 Ma) in sample DB03 of Bradley et al. (2022), the Atilis Quartzite Formation could be Ediacaran in age in agreement with the overlying formations of the Oumachoueima Group. Nonetheless, the isolated and single youngest dates (c. 707 Ma in sample AKJ16 and c. 593 Ma in sample DB03; Fig. 6b) were not replicated in any of the other three samples of the Atilis Quartzite Formation. Furthermore, none of the samples of the Atilis Quartzite Formation show the characteristic late

Cryogenian–Ediacaran (i.e., Brasiliano /Pan-African orogenies; see section 5.2) peak typical of other Ediacaran or younger rocks in the region. We conclude hence that the two isolated and single youngest dates are geologically meaningless and likely due to some analytical anomaly and/or undetected Pb loss. Therefore, we propose that the Atilis Quartzite Formation is indeed of early Tonian age, as suggested by its MDAs, and correlates with the Assabet el Hassiane Group of the Taoudeni Basin (see section 5.2.2.). This interpretation suggests a prolonged sedimentary gap (c. 300 Ma) between the deposition of the Atilis Quartzite Formation and the overlying Ediacaran formations of the Oumachoueima Group.

A closer examination of the samples from the Atomai and Sainte Barbe formations shows some differences between them (Fig. 6b). The two samples from the Atomai Formation yielded middle Ediacaran MDAs (c. 595 Ma and 586 Ma), while the five samples from the Sainte Barbe Formation yielded latest Ediacaran-early Cambrian MDAs (c. 566-534 Ma) (Fig. 6b). These younger MDAs upwards in the sedimentary succession can be interpreted as reflecting the TDAs. This interpretation is supported by the abundant felsic and mafic volcanic rocks intercalated in the Oumachoueima Group (with the exception of the Atilis Quartzite Formation). This widespread late Cryogenian to early Cambrian magmatism is related to the Brasiliano/Pan-African orogenies and their latest magmatic pulses, as well-documented in and around West Africa and Amazonia (e.g., Grenholm et al., 2019; Condie et al., 2009; Chew et al., 2008) (Fig. 6a). The persistent volcanism in the Choueima nappe of the Inchiri Complex would likely act as a local source of newformed zircon grains, which would have been incorporated into the coeval sediments, thus giving way to younger ages (TDA) upwards in the succession. Interestingly, the youngest peak, formed by three grains from sample CT02 from Bradley et al. (2022), indicates an MDA of approximately 534 Ma and establishes an early Cambrian age at least for the uppermost strata of the Sainte Barbe Formation.

Regarding the Nouatil Group, an age constraint comes from U-Pb dating of zircon grains in a basal tuff of the underlying Teniagouri Group in the Taoudeni Basin (Bradley et al., 2015), which yielded a CA-TIMS zircon age of 569.37 \pm 0.36 Ma. This suggests that the base of the Nouatil Group cannot be older than the late Ediacaran (Pitfield et al., 2004) and agrees with the MDA obtained from our sample (AKJ1, c. 613 Ma). Furthermore, sample DB28 from the Nouatil Group in the Adrar region studied by Bradley et al. (2022) yielded a younger MDA (c. 543 Ma), in accordance with the early Cambrian age suggested for this group (Pitfield et al., 2004; Bradley et al., 2015).

5.2. Sediment sources in the northern Mauritanide Belt

Provenance studies supported by statistical analyses of detrital zircon age distributions are based on comparing the age spectra of (meta)sedimentary samples with those of potential source areas (see for instance Fedo et al. (2003) and references therein). Fig. 6a shows the detrital zircon age spectra of the samples in the Akjoujt area (this work and Bradley et al., 2022). Two types of detrital zircon age distributions (I and II) have been identified.

Type I age spectra appear in samples of the Agoualilet Unit (AKJ33) and upper Oumachoueima Group (AKJ5, CT21, AKJ14, DB01, CT02, AKJ11) and shows a main late Cryogenian-Ediacaran population (c. 680–540 Ma), a minor Rhyacian–Orosirian population (c. 2.2–1.9 Ga), and occasional Mesoarchean–Neoarchean ages (c. 3.0–2.5 Ga). Primary sources of these ages are well known in the WAC (see compilation in Fig. 6a), and correspond to the Pan-African, Eburnean and Leonian–Liberian orogenies (Nance et al., 2008; Ustaömer et al., 2011; Linnemann et al., 2012). Importantly, the typical WAC signature does not include ages in the range c. 1.9–0.9 Ga (Mesoproterozoic gap). However, some of the type I age spectra samples (CT21 and AKJ14) contain a minor but noticeable number (up to 12.9 % of the data) of Mesoproterozoic detrital zircon grains (see sub-section 5.2.1. below).

Type II age spectra are attested by samples of the Oumachoueima

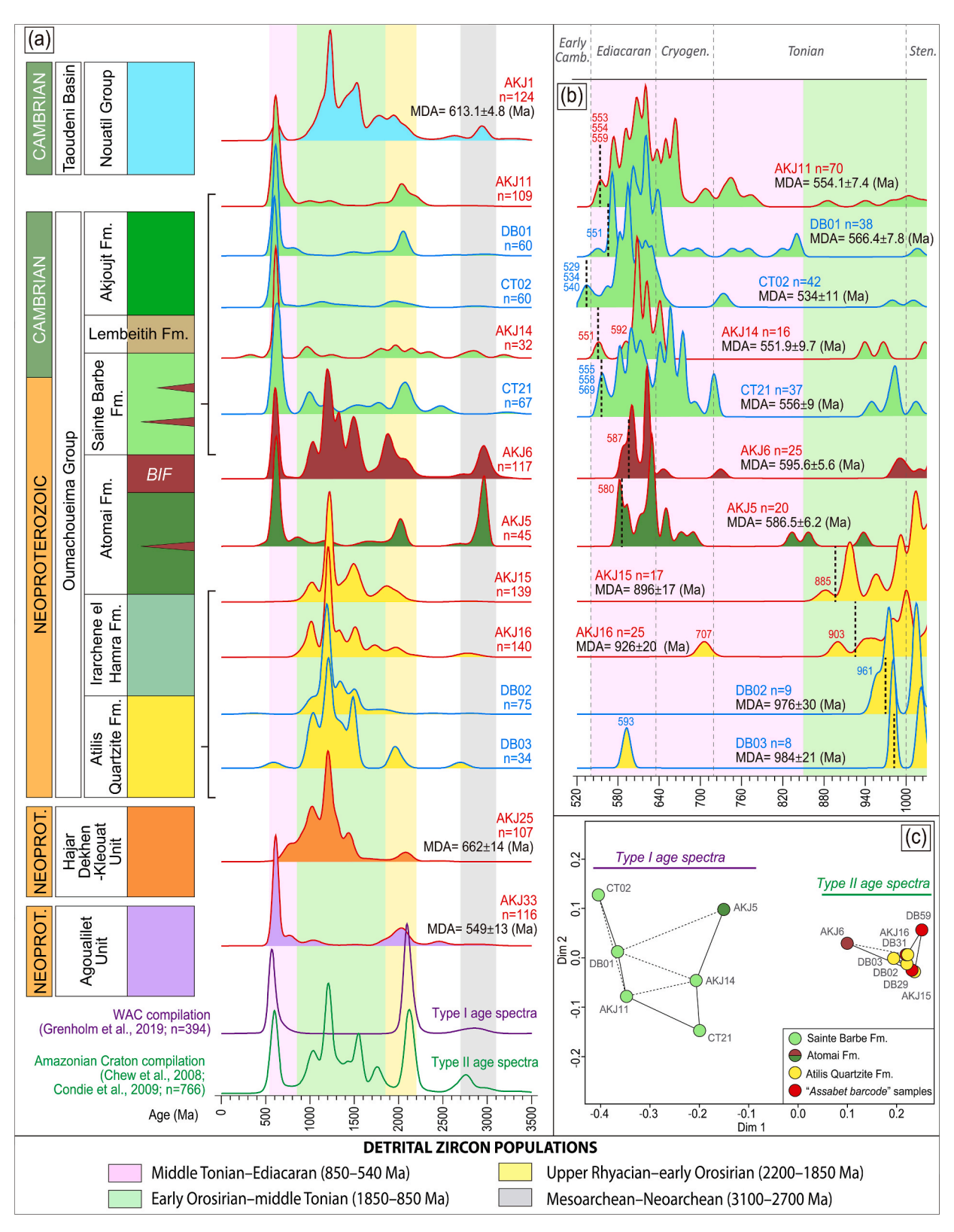


Fig. 6. Comparison of KDE plots for the different tectonostratigraphic units in the Akjoujt area. a) Complete age spectra (0–3500 Ma). b) Middle Stenian–Cambrian spectra (1100–520 Ma). Red lines represent the samples from this study, while blue lines correspond to data from Bradley et al. (2022). Vertical discontinuous black lines in (b) indicate the MDA of each sample, while isolated numbers refer to the youngest zircon ages in each sample. The KDE plots, based on regional compilations of igneous and detrital zircon ages from the WAC and Amazonian Craton (see references in the figure), represent the characteristic signature of these source areas, serving as a pattern for comparison (type I and type II age spectra). c) Multidimensional Scaling analysis (MDS) (Vermeesch, 2013) diagram showing the dissimilarities between samples from the Oumachoueima Group, based on data from this study and Bradley et al. (2022). IsoplotR is used to calculate MDS distances and produce the plot. The closest neighbors are indicated with a continuous line, whereas the second-closest ones are indicated with a discontinuous line. The red dots (samples DB29, DB59 and DB31) represent samples from the Taoudeni Basin in the Adrar region reported by Bradley et al. (2022), which show type II age spectra, also referred to as the "Assabet barcode" in that study.

Group (Atilis Quartzite Formation and sample AKJ6 from the upper Atomai Formation), Hajar Dekhen Unit (AKJ25) and Nouatil Group (AKJ1). The detrital zircon age distribution of these samples includes the same populations as type I (with or without the Cryogenian-Ediacaran peak), but it incorporates a dominant population within the range of ages from c. 1.9 to 0.9 Ga (Mesoproterozoic s.l.; Fig. 6a). As previously stated, these Mesoproterozoic s.l. ages are virtually absent in the WAC, but they are common in the Baltican, Laurentian, and Amazonian cratons (Bradley et al., 2022). According to the available paleogeographic reconstructions (e.g., Robert et al. (2021) and references therein), during most of the Neoproterozoic period Amazonia was close or connected to the WAC, whereas Laurentia and Baltica were separated from the WAC and Amazonia by large oceanic realms because of Rodinia breakup. Consequently, the most plausible primary sediment source for type II detrital zircon spectra in the Akjoujt area points to Amazonia, as already proposed by Bradley et al. (2022). The Amazonian basement is characterized by Cryogenian-Cambrian ages (c. 720-500 Ma), associated with the Brasiliano Orogeny, and Statherian-early Tonian (c. 1.8-0.9 Ga, Mesoproterozoic s.l.) ages linked to the Rio Negro-Juruena (c. 1.8-1.55 Ga), Rondonian-San Ignacio (c. 1.55-1.3 Ga), and Sunsás-Grenvillian (c. 1.3-0.9 Ga) orogenies (Nance et al., 2008; Ustaömer et al., 2011; Linnemann et al., 2012). Additionally, Rhyacian-Orosirian ages (c. 2.2-1.9 Ga) associated with the Trans-Amazonian Orogeny, and Neoarchean ages (c. 2.8-2.5 Ga) linked to the Central Amazonian Orogeny are also common. Most of these Amazonian ages are present in type II detrital zircon age spectra (Fig. 6a). In particular, peak ages corresponding to the Sunsás-Grenvillian, Rondonian-San Ignacio, Transand Central-Amazonian orogenies are globally interpreted as indicative of provenance from the Amazonian Craton (Nance et al., 2008; Ustaömer et al., 2011).

The Hajar Dekhen-Kleouat Unit (sample AKJ25) is akin to type II detrital zircon age distribution. This unit is exposed in allochthonous klippes lying onto the Choueima nappe (Pitfield et al., 2004; Bradley et al., 2015) and has Ediacaran TDA (c. 662–559 Ma; see section 5.1). We hypothesize that the Hajar Dekhen-Kleouat Unit might represent a terrane very distal or external to the WAC, with a sedimentary cover akin to Amazonia and a strong Ediacaran (Brasiliano and/or Pan-African) magmatic imprint. Nonetheless, the relationships between the Hajar Dekhen-Kleouat, Saouda, and Agoualilet units are unknown, and hence our hypothesis remains a speculation.

5.2.1. Detrital zircon source variation in the Oumachoueima Group and correlation with the Taoudeni Basin

The metasedimentary rocks of the Oumachoueima Group display variability in their zircon age spectra, with alternance of types I and II in the sampled succession (Fig. 6a). This variability is also observed in a Multidimensional Scaling (MDS) plot (Fig. 6c), which, using Kolmogorov-Smirnov statistics, allows for the comparison of dissimilarities among multiple samples, clustering the most similar ones and separating the most dissimilar ones (Vermeesch, 2013).

The new data from the Atilis Quartzite Formation do not differ from those previously reported by Bradley et al. (2022) for the same formation (samples DB02 and DB03) (Fig. 6a), thus reinforcing the interpretation that Amazonia was the primary source of the Tonian basal deposits of the Oumachoueima Group, when the Inchiri Complex was likely connected to both the WAC and the Amazonian Craton in the Rodinia supercontinent (Robert et al., 2021) (Figs. 7 and 8). The detrital zircon record of the overlying Ediacaran Atomai Formation (sample AKJ5) reveals a clear affinity to type I age spectra and WAC provenance. In particular, the nearby Amsaga basement (including the c. 2.9 Ga Aoutitilt and Arhdéjit granites; Pitfield et al., 2004), which constitutes the autochthonous basement of the Choueima nappe, might be the source of the relatively abundant c. 2.9 Ga detrital zircon grains in this sample. By contrast, the iron-rich sandstone (AKJ6) collected close to the top of the Atomai Formation includes the same populations recorded by sample AKJ5 plus a continuous distribution of data in the interval c.

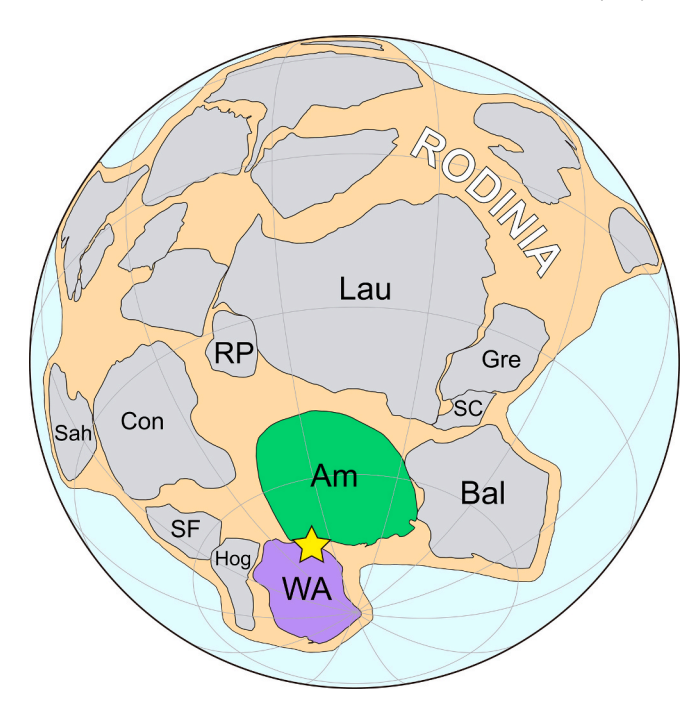


Fig. 7. Paleogeographic reconstruction of the supercontinent Rodinia at 900 Ma (modified from Robert et al., 2021). Abbreviations: Am (Amazonia), Bal (Baltica), Con (Congo), Gre (Greenland), Hog (Hoggar), Lau (Laurentia), RP (Rio de la Plata), Sah (Sahara), SC (Scotland-Ireland), SF (São Francisco), WA (West Africa). The cratons of interest in this study are shown in purple (West African) and green (Amazonian). The star indicates the inferred position of the studied area.

1.9–1.0 Ga, with peaks comparable with those described for the Atilis Quartzite Formation (Fig. 6a). Thus, the overall zircon content of sample AKJ6 is akin to type II distribution, suggesting an Amazonian affinity for the sedimentary rocks of the upper part of the Atomai Formation. Finally, the detrital zircon signature identified in the Sainte Barbe Formation is type I, suggesting a WAC affinity for this unit.

The changes in the detrital zircon record throughout the Oumachoueima Group succession might be interpreted as resulting from shifts in drainage systems, and the subsequent opening of an oceanic realm at late Ediacaran time in between the WAC and the Amazonian Craton (the so-called Clymene Ocean; Robert et al. (2021) and references therein) (Fig. 8) (see discussion in section 5.3 below).

The Neoproterozoic–early Cambrian succession of the Taoudeni Basin in the Adrar region (Assabet el Hassiane, Jbeliat, Teniagouri, and partially the Nouatil groups) contains detrital zircon signatures dominated by Mesoproterozoic populations (Bradley et al., 2022). However, the extent to which these populations derive from primary sources or represent inherited signatures has not been previously discussed.

Our proposal of a Tonian age for the Atilis Quartzite Formation coincides with the age assigned to the Assabet el Hassiane Group of the Taoudeni Basin (Bradley et al., 2022). The Assabet el Hassiane group is the oldest with a distinctive and uncommon detrital zircon age distribution in the WAC, referred to as the 'Assabet barcode' by Bradley et al. (2022). Interestingly, this barcode matches the Mesoproterozoic age compilation for Amazonian Craton (Fig. 6a) and the detrital zircon signature obtained in this study for the Atilis Quartzite samples (Fig. 6c). Therefore, we consider the Assabet el Hassiane Group to be stratigraphically equivalent to the Atilis Quartzite Formation, although deposited in more internal zones of the WAC (Taoudeni Basin), and thus it would have recorded a primary Mesoproterozoic signal through drainage systems within the Rodinia supercontinent, where the WAC and Amazonia were connected (c. 900 Ma, Figs. 7 and 8).

Overlying the Assabet el Hassiane Group, the Jbeliat and Teniagouri groups partially reproduce the 'Assabet barcode' (Bradley et al., 2022).

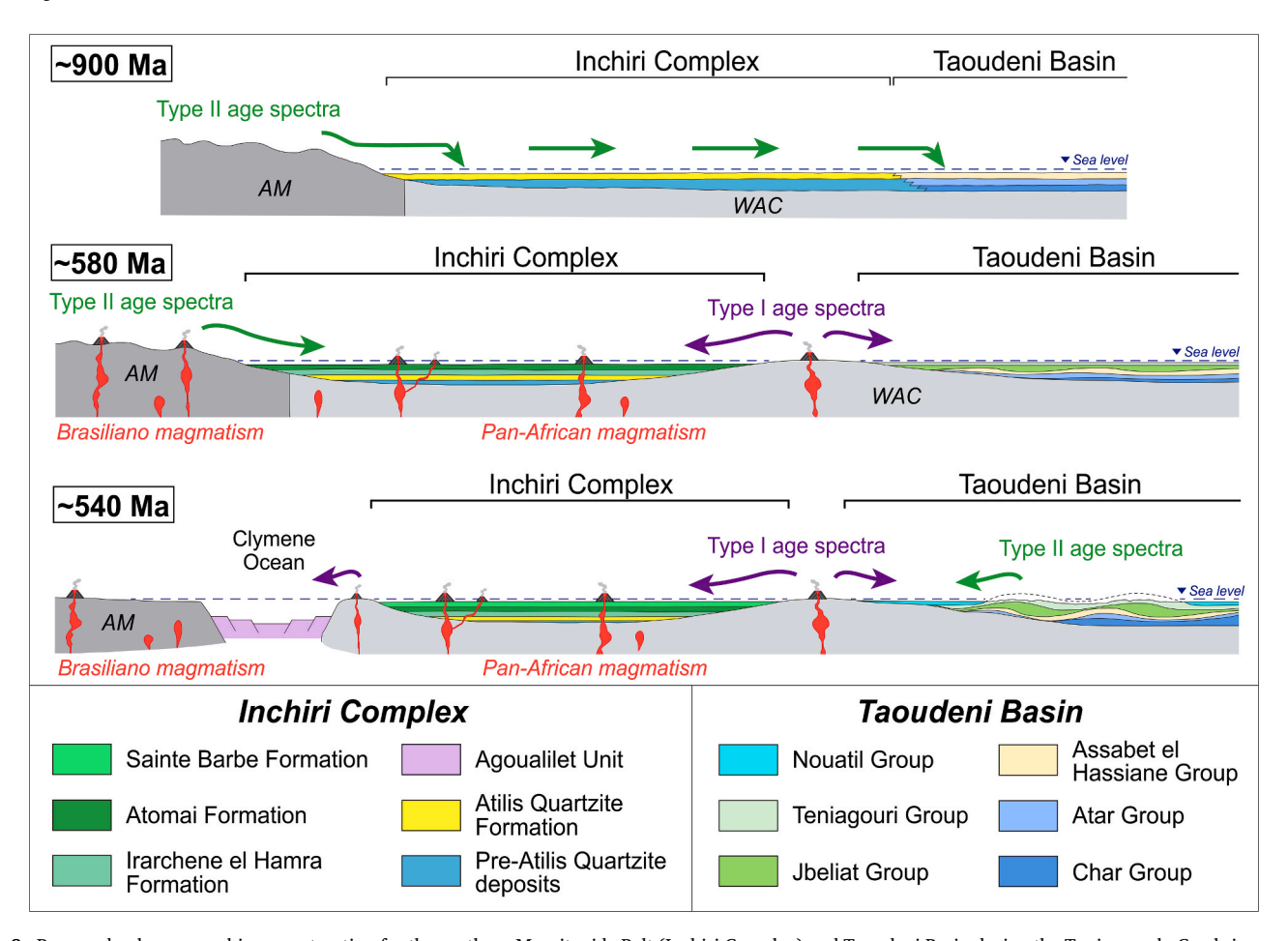


Fig. 8. Proposed paleogeographic reconstruction for the northern Mauritanide Belt (Inchiri Complex) and Taoudeni Basin during the Tonian–early Cambrian period (c. 900–540 Ma). Abbreviations: AM (Amazonian Craton), WAC (West African Craton).

Since these groups are separated by regional unconformities (Moussine-Pouchkine and Bertrand-Sarfati, 1997; Pitfield et al., 2004; Deynoux et al., 2006), their Mesoproterozoic detrital zircon populations could be the result of sedimentary recycling of the underlying formations.

Based on the Cambrian age assigned to the Nouatil Group, the dominant Mesoproterozoic detrital zircon signature in the sample AKJ1 must be recycled from an intermediate repository, since the WAC and the Amazonian Craton were already separated by the Clymene oceanic realm at late Ediacaran time (c. 550-540 Ma) (see section 5.3), which prevented a primary Amazonian source. Nevertheless, alternative explanations other than an intervening ocean might also be considered, as for instance crustal subsidence in the source areas (Amazonia) and/or sea level rise (Fig. 8). Whatever the case, we propose that the Mesoproterozoic detrital zircon grains recorded in the Nouatil Group sample come from the recycling of older, 'Assabet barcode' bearing sediments in the Taoudeni Basin (Fig. 8). These sedimentary rocks were eroded during the early Cambrian, as evidenced by the unconformity between the Teniagouri Group and the Nouatil Group in the Adrar region (Pitfield et al., 2004). As for the minor Ediacaran population in sample AKJ1, it could be either recycled from the Teniagouri Group or derived from a primary Pan-African volcanic source.

In the Inchiri Complex, the late Ediacaran–early Cambrian Sainte Barbe Formation would be coeval to the Teniagouri or Nouatil groups. Although the detrital zircon signature of the Sainte Barbe Formation is of type I (akin to WAC basement) (Fig. 6a), its scarce yet noticeable Mesoproterozoic zircon grains can be interpreted also as recycled from older sedimentary rocks of the Taoudeni Basin.

5.3. Neoproterozoic tectonic and paleogeographic setting of the northern Mauritanide Belt

The detrital zircon record of sedimentary basins represents a fundamental archive for geodynamic processes, such as formation of new lithosphere and crustal recycling. Nevertheless, inferring the tectonic setting of ancient sedimentary basins is not straightforward. In this regard, Cawood et al. (2012) proposed an approach based on cumulative detrital zircon age distributions. However, ambiguity in the interpretation of his tectonic discrimination diagram arises from overlapping fields and/or TDA uncertainty. More recently, Barham et al. (2022) have proposed a new statistical method based on the age difference between the 10th and 50th percentiles of the detrital zircon age distribution, and a modified chi-squared analysis of age population modality and dispersion. This method results in an "age distribution fingerprint" that allows distinguishing between divergent (rift/passive margin) and convergent (subduction/collision) tectonic settings (Fig. 9). In contrast with Cawood's et al. (2012) method, this new approach can be applied also in those cases, such as our study, in which the TDAs are not well constrained. Fig. 9 shows our detrital zircon samples plotted using Barham's et al. (2022) method, and how they consistently fall in the divergent setting field.

Unfortunately, there are no systematic geochemical studies focused on the tectonic setting of the late Neoproterozoic magmatic rocks of the northern Mauritanide Belt. The only scarce and limited geochemical data available come from metabasalts intercalated in the Akjoujt Formation. This data suggests that the volcanism was tholeitic and with MORB affinity (Pitfield et al., 2004). However, in most areas where this magmatism is well characterized from a geochemical point of view, the

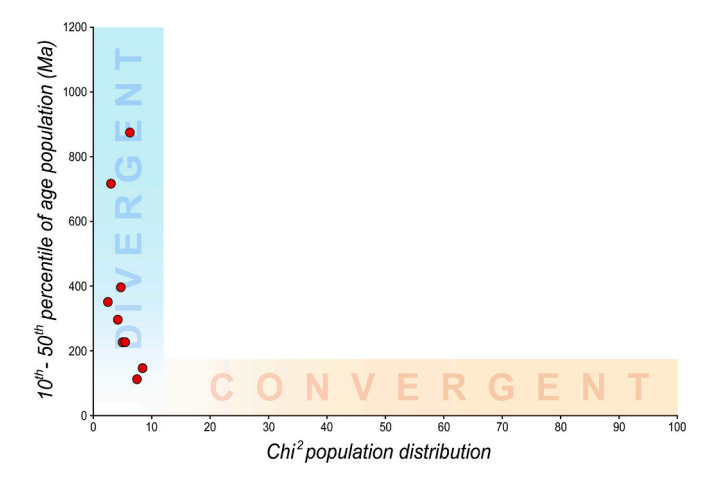


Fig. 9. Bivariate discrimination plot of active convergent versus divergent/passive margins applied in this study, based on the metrics defined by Barham et al. (2022). The red dots represent the samples from this study.

widely accepted large-scale scenario for the late Cryogenian to early Cambrian time span is a subduction/collision-related one (Pan-African/Brasiliano orogenies; e.g., Nance et al., (2008) and references therein). This magmatism partially overlaps with the late Ediacaran–Cambrian magmatic arc that developed along the northern Gondwana margin (Avalonian/Cadomian subduction-related arc; see inset in Fig. 1a; Murphy et al., 2004; Linnemann et al., 2008; Garfunkel, 2015). In this context, bimodal magmatism and crustal extension (including the development of small-scale oceanic realms) in adjacent regions have been interpreted as related to back-arc extension governed by Avalonian/Cadomian subduction slab retreat (e.g., Oriolo et al., 2021 and references therein).

Alternatively, a rifting setting has also been proposed for adjacent sectors to the one studied here. In this regard, the Oulad Dlim (or Soutufide Belt) Massif (Western Sahara), which is the northward continuation of the Mauritanide Belt (Fig. 1a–b), also contains voluminous bimodal Ediacaran magmatism, which has been recently related to an intracontinental rift setting (Bea et al., 2020). This proposal is based on a wealth of geochemical and isotopic data, which substantially differs from those diagnostic of exhumed ancient magmatic arcs (Bea et al., 2020).

Based on the above arguments, the late Neoproterozoic sedimentary successions in the northern Mauritanide Belt units can be tentatively better explained within the context of a magma-rich continental rift, developed along the western margin (in present-day coordinates) of the WAC and adjacent to the neighboring Amazonian Craton (Figs. 7 and 8). Our study supports the interpretation that both cratons constituted source areas for the Neoproterozoic basins of the northern Mauritanide Belt until late Ediacaran time (c. 550 Ma), when a relatively small oceanic domain, namely the Clymene Ocean, separated the WAC from the Amazonian Craton. In this regard, the sample analyzed from the ophiolitic-like Agoulalitet Unit (sample AKJ33), with a MDA of c. 550 Ma, might attest the initial oceanization stages. The Clymene Ocean was likely short-lived and closed up a few million years later, leading to the assembly of Gondwana by the early Cambrian.

6. Conclusions

New U-Pb detrital zircon dates from nine (meta)sandstone samples constrain the stratigraphy and sediment provenance of the Neoproterozoic–Cambrian successions in the northern Mauritanide Belt sector. Two detrital zircon age spectra alternate among the different formations in this region: type I derives from the WAC and features a main late Cryogenian–Ediacaran complex population, with a second-order Rhyacian–Orosirian population and scattered

Mesoarchean–Neoarchean ages; type II primarily derives from Amazonian Craton sources and is characterized by the same populations as type I, plus an outstanding Mesoproterozoic s.l. population (c. 1.9–0.9 Ga).

The oldest metasedimentary rocks sampled in the northern Mauritanide Belt sector are those of the Atilis Quartzite Formation of the Oumachoueima Group, which are attributed here to the early Tonian based on maximum depositional age. This formation yielded a dominant Mesoproterozoic detrital input, primarily derived from the Amazonian Craton, which has been also reported in the Assabet el Hassiane Group of the intracratonic Taoudeni Basin that covers the interior of the WAC. Thus, a stratigraphic correlation of the Atilis Quartzite Formation and the Assabet el Hassiane Group is proposed. The Mesoproterozoic Amazonian Craton-derived detrital zircon signal has also been found in the Cryogenian strata of the allochthonous Hajar Dekhen-Kleouat Unit, largely intruded by Pan-African porphyritic granites.

Following a sedimentary gap of c. 300 Ma, the middle Ediacaran Atomai Formation of the Oumachoueima Group records both the Amazonian Craton and WAC (Mesoproterozoic free) signatures. The record of the overlying Sainte Barbe Formation, late Ediacaran to early Cambrian in age, does not include primarily derived Amazonian Craton detrital zircon grains. This was likely due to the opening of a short-lived oceanic realm (the Clymene Ocean, likely represented by the ophiolite-like Agoualilet Unit) by c. 550 Ma, between the Amazonian Craton and the WAC. Despite the latest Ediacaran drift of the Amazonian Craton, the Mesoproterozoic detrital signal persisted in the Cambrian sedimentation of the Taoudeni Basin (Nouatil Group) through recycling of the underlying succession.

Overall, the Neoproterozoic sedimentary evolution of the northern Mauritanide Belt envisages a paleogeographic link between the Amazonian and the West African cratons since Rodinia amalgamation. This connection was interrupted during the latest Ediacaran through the development of the short-lived Clymene oceanic realm.

Data availability

The supporting data for this work, including U-Pb data (Supplementary Data S1) and Wetherill diagrams (Supplementary Data S2) are available from the Mendeley Data repository (https://doi.org/10.17632/5275gnn9p3.1; https://doi.org/10.17632/drvm49prwj.1).

CRediT authorship contribution statement

Roberto Jiménez Borrego: Writing – review & editing, Writing – original draft, Visualization, Software, Methodology, Investigation, Formal analysis, Data curation, Conceptualization. David Martínez Poyatos: Writing – review & editing, Writing – original draft, Validation, Supervision, Project administration, Investigation, Funding acquisition, Conceptualization. Antonio Azor: Writing – review & editing, Writing – original draft, Validation, Supervision, Investigation, Conceptualization. Cristina Accotto: Writing – review & editing, Writing – original draft, Validation, Supervision, Investigation, Formal analysis, Conceptualization. Antonio Jabaloy-Sánchez: Writing – review & editing, Investigation, Conceptualization. Francisco González Lodeiro: Resources. Mohamed Salem Sabar: Resources. Ahmed Hamoud: Resources. Ahmed Ould Ely Lekouyrie: Resources.

Declaration of Competing Interest

The authors declare that they have no known competing financial interests or personal relationships that could have appeared to influence the work reported in this paper.

Acknowledgements

This research was financed by the Spanish Ministry of Science and Innovation (MICIN) and the State Research Agency (AEI, 10.13039/

501100011033) through the project TARDIVARI (PID2020-118822GB-I00) and the pre-doctoral scholarship PRE2021-098050. Funding for open access charge: University of Granada/CBUA. We are indebted to Noreen Evans, for her assistance and technical support on sample preparation and LA-ICPMS analysis. Comments from one anonymous reviewer and Prof. Sebastián Oriolo are acknowledged and greatly appreciated. Their constructive feedback helped to improve the quality of the manuscript. Editorial handling by Prof. Andrea Festa is also gratefully acknowledged.

Appendix A. Supplementary data

Supplementary data to this article can be found online at https://doi.org/10.1016/j.gr.2025.07.026.

References

- Ait Lahna, A., Youbi, N., Tassinari, C.C.G., Basei, M.A.S., Ernst, R.E., Chaib, L., Barzouk, A., Mata, J., Gärtner, A., Admou, H., Boumehdi, M.A., Söderlund, U., Bensalah, M.K., Bodinier, J.-L., Maacha, L., Bekker, A., 2020. Revised stratigraphic framework for the lower Anti-Atlas Supergroup based on U-Pb geochronology of magmatic and detrital zircons (Zenaga and Bou Azzer-El Graara inliers, Anti-Atlas Belt, Morocco). J. Afr. Earth Sci. 171, 103946. https://doi.org/10.1016/j.iafrearsci.2020.103946.
- Albert-Villanueva, E., Permanyer, A., Tritlla, J., Levresse, G., Salas, R., 2016. Solid hydrocarbons in proterozoic dolomites, Taoudeni Basin, Mauritania. J. Pet. Geol. 39, 5–27. https://doi.org/10.1111/jpg.12625.
- Andersen, T., Elburg, M.A., Magwaza, B.N., 2019. Sources of bias in detrital zircon geochronology: Discordance, concealed lead loss and common lead correction. Earth Sci. Rev. 197, 102899. https://doi.org/10.1016/j.earscirev.2019.102899.
- Barham, M., Kirkland, C.L., Handoko, A.D., 2022. Understanding ancient tectonic settings through detrital zircon analysis. Earth Planet. Sci. Lett. 583, 117425. https://doi.org/10.1016/j.epsl.2022.117425.
- Bea, F., Montero, P., Haissen, F., Molina, J.F., Lodeiro, F.G., Mouttaqi, A., Kuiper, Y.D., Chaib, M., 2020. The Archean to Late-Paleozoic architecture of the Oulad Dlim Massif, the main Gondwanan indenter during the collision with Laurentia. Earth Sci. Rev. 208, 103273. https://doi.org/10.1016/j.earscirev.2020.103273.
- Bradley, D.C., Evans, D.A.D., O'Sullivan, P., Taylor, C.D., Eglington, B.M., 2022. The Assabet barcode: Mesoproterozoic detrital zircons in Neoproterozoic strata from Mauritania, West Africa. Am. J. Sci. 322, 939–992. https://doi.org/10.2475/ 08.2023.01
- Bradley, D.C., ÓSullivan, P., Cosca, M.A., Motts, H.A., Horton, J.D., Taylor, C.D., Beaudoin, G., Lee, G.K., Ramezani, J., Bradley, D.B., Jones, J. V., Bowring, S., 2015. Synthesis of geological, structural, and geochronologic data (phase V, deliverable 53), chapter A, in Taylor, C. D., editor., Second projet de renforcement institutionnel du secteur minier de la République Islamique de Mauritanie (PRISM-II): U.S. Geol. Surv. Open-File Rep. 2013–1280-A, 140 p. doi: 10.3133/ofr20131280.
- Cawood, P.A., Hawkesworth, C.J., Dhuime, B., 2012. Detrital zircon record and tectonic setting. Geology 40, 875–878. https://doi.org/10.1130/G32945.1.
- Chew, D., Magna, T., Kirkland, C., Miskovic, A., Cardona, A., Spikings, R., Schaltegger, U., 2008. Detrital zircon fingerprint of the Proto-Andes: Evidence for a Neoproterozoic active margin? Precambrian Res. 167, 186–200. https://doi.org/ 10.1016/j.precamres.2008.08.002.
- Condie, K.C., Belousova, E., Griffin, W.L., Sircombe, K.N., 2009. Granitoid events in space and time: Constraints from igneous and detrital zircon age spectra. Gondwana Res. 15, 228–242. https://doi.org/10.1016/j.gr.2008.06.001.
- Cordani, U.G., Brito-Neves, B.B., D'Agrella-Filho, M.S., 2003. From Rodinia to Gondwana: A Review of the Available Evidence from South America. Gondwana Res. 6, 275–283. https://doi.org/10.1016/S1342-937X(05)70976-X.
- Coutts, D.S., Matthews, W.A., Hubbard, S.M., 2019. Assessment of widely used methods to derive depositional ages from detrital zircon populations. Geosci. Front. 10, 1421–1435. https://doi.org/10.1016/j.gsf.2018.11.002.
- Dallmeyer, R.D., Lécorché, J.P., 1989. 40Ar/39Ar polyorogenic mineral age record within the central Mauritanide orogen, West Africa. Geol. Soc. Am. Bull. 101, 55–70. https://doi.org/10.1130/0016-7606(1989)101<0055:AAPMAR>2.3.CO;2.
- Deynoux, M., Affaton, P., Trompette, R., Villeneuve, M., 2006. Pan-African tectonic evolution and glacial events registered in Neoproterozoic to Cambrian cratonic and foreland basins of West Africa. J. Afr. Earth Sci. 46, 397–426. https://doi.org/ 10.1016/j.jafrearsci.2006.08.005.
- Fedo, C.M., Sircombe, K.N., Rainbird, R.H., 2003. Detrital Zircon Analysis of the Sedimentary Record. Rev. Mineral. Geochem. 53, 277–303. https://doi.org/ 10.2113/0520277
- Foster, D.A., Goscombe, B.D., Newstead, B., Mapani, B., Mueller, P.A., Gregory, L.C., Muvangua, E., 2015. U-Pb age and Lu-Hf isotopic data of detrital zircons from the Neoproterozoic Damara Sequence: Implications for Congo and Kalahari before Gondwana. Gondwana Res. 28, 179-190. https://doi.org/10.1016/j. gr.2014.04.011.
- Garfunkel, Z., 2015. The relations between Gondwana and the adjacent peripheral Cadomian domain—constrains on the origin, history, and paleogeography of the peripheral domain. Gondwana Res. 28, 1257–1281. https://doi.org/10.1016/j. gr.2015.05.011.

Grenholm, M., Jessell, M., Thébaud, N., 2019. A geodynamic model for the Paleoproterozoic (ca. 2.27-1.96 Ga) Birimian Orogen of the southern West African Craton – Insights into an evolving accretionary-collisional orogenic system. Earth. Sci. Rev. 192, 138-193. https://doi.org/10.1016/j.earscirev.2019.02.006.

- Jackson, S.E., Pearson, N.J., Griffin, W.L., Belousova, E.A., 2004. The application of laser ablation-inductively coupled plasma-mass spectrometry to in situ U-Pb zircon geochronology. Chem. Geol. 211, 47–69. https://doi.org/10.1016/j. chemgeo. 2004.06.017
- Kalsbeek, F., Frei, D., Affaton, P., 2008. Constraints on provenance, stratigraphic correlation and structural context of the Volta basin, Ghana, from detrital zircon geochronology: An Amazonian connection? Sediment. Geol. 212, 86–95. https://do. org/10.1016/j.sedgeo.2008.10.005.
- Keppie, J.D., Nance, R.D., Murphy, J.B., Dostal, J., 2003. Tethyan, Mediterranean, and Pacific analogues for the Neoproterozoic–Paleozoic birth and development of peri-Gondwanan terranes and their transfer to Laurentia and Laurussia. Tectonophysics 365, 195–219. https://doi.org/10.1016/S0040-1951(03)00037-4.
- Key, R.M., Loughlin, S.C., Gillespie, M., Del Rio, M., Horstwood, M.S.A., Crowley, Q.G., Darbyshire, D.P.F., Pitfield, P.E.J., Henney, P.J., 2008. Two Mesoarchaean terranes in the Reguibat shield of NW Mauritania. Geol. Soc. Lond. Spec. Publ. 297, 33–52. https://doi.org/10.1144/SP297.3.
- Le Goff, É., Guerrot, C., Maurin, G., Johan, V., Tegyey, M., Ben Zerga, M., 2001. Découverte d'éclogites hercyniennes dans la chaîne septentrionale des Mauritanides (Afrique de l'Ouest). C. R. Acad. Sci. - Series IIA - Earth Planet. Sci. 333, 711–718. https://doi.org/10.1016/S1251-8050(01)01694-9.
- Lécorché, J.P., Clauer, N., 1984. First radiometric date (K/Ar) on the front of the Mauritanides in the Akjoujt region (Mauritania). In: The Caledonian Orogen and Palaeozoic Orogenesis (R. Hayot En-Noufous, ed.). IGCP Project 27 Symposium Morocco, Rabat, 23.
- Linnemann, U., Herbosch, A., Liégeois, J.-P., Pin, C., Gärtner, A., Hofmann, M., 2012. The Cambrian to Devonian odyssey of the Brabant Massif within Avalonia: A review with new zircon ages, geochemistry, Sm-Nd isotopes, stratigraphy and palaeogeography. Earth. Sci. Rev. 112, 126–154. https://doi.org/10.1016/j.earscirey.2012.02.007
- Linnemann, U., Pereira, F., Jeffries, T.E., Drost, K., Gerdes, A., 2008. The Cadomian Orogeny and the opening of the Rheic Ocean: The diacrony of geotectonic processes constrained by LA-ICP-MS U-Pb zircon dating (Ossa-Morena and Saxo-Thuringian Zones, Iberian and Bohemian Massifs). Tectonophysics 461, 21–43. https://doi.org/ 10.1016/j.tecto.2008.05.002.
- Marcelin, J., 1968. Carte géologique de la région d'Akjoujt.
- Marsh, J.H., Jørgensen, T.R.C., Petrus, J.A., Hamilton, M.A., Mole, D.R., 2019. U-Pb, trace element and hafnium isotope composition of the Maniitsoq zircon: A potential new Archean zircon reference material. Goldschmidt Abstr. 2161.
- Martyn, J., Strickland, C., 2004. Stratigraphy, structure and mineralisation of the Akjoujt area. Mauritania. J. Afr. Earth Sci. 38, 489–503. https://doi.org/10.1016/j. jafrearsci.2004.03.004.
- McGee, B., Babinski, M., Trindade, R., Collins, A.S., 2018. Tracing final Gondwana assembly: Age and provenance of key stratigraphic units in the southern Paraguay Belt, Brazil. Precambrian Res. 307, 1–33. https://doi.org/10.1016/j. precamres.2017.12.030.
- Moussine-Pouchkine, A., Bertrand-Sarfati, J., 1997. Tectonosedimentary subdivisions in the neoproterozoic to Early Cambrian cover of the taoudenni Basin (Algeria-Mauritania-Mali). J. Afr. Earth Sci. 24, 425–443. https://doi.org/10.1016/S0899-5365(97)00073-0
- Murphy, J.B., Pisarevsky, S.A., Nance, R.D., Keppie, J.D., 2004. Neoproterozoic?Early Paleozoic evolution of peri-Gondwanan terranes: implications for Laurentia-Gondwana connections. Int. J. Earth Sci. 93, 659–682. https://doi.org/10.1007/ s00531-004-0412-9.
- Nance, R.D., Murphy, J.B., Strachan, R.A., Keppie, J.D., Gutiérrez-Alonso, G., Fernández-Suárez, J., Quesada, C., Linnemann, U., D'lemos, R., Pisarevsky, S.A, 2008.
 Neoproterozoic-Early Palaeozoic tectonostratigraphy and palaeogeography of the peri-Gondwanan terranes: Amazonian v. West African connections. Geol. Soc. Lond. Spec. Publ. 297, 345–383. https://doi.org/10.1144/SP297.17.
- Oriolo, S., Schulz, B., Geuna, S., González, P.D., Otamendi, J.E., Sláma, J., Druguet, E., Siegesmund, S., 2021. Early Paleozoic accretionary orogens along the Western Gondwana margin. Geosci. Front. 12, 109–130. https://doi.org/10.1016/j.gsf.2020.07.001.
- Pereira, M.F., Gama, C., 2021. Revisiting the Intermediate Sediment Repository Concept Applied to the Provenance of Zircon. Minerals 11, 233. https://doi.org/10.3390/ min11030233.
- Pisarevsky, S.A., Elming, S.-Å., Pesonen, L.J., Li, Z.-X., 2014. Mesoproterozoic paleogeography: Supercontinent and beyond. Precambrian Res. 244, 207–225. https://doi.org/10.1016/j.precamres.2013.05.014.
- Pitfield, P.E.J., Key, R.M., Waters, C.N., Hawkins, M.P.H., Schofield, D.I., Loughlin, S., Barnes, R.P., 2004. Notice explicative des cartes géologiques et gîtologiques à 1/200 000 et 1/500 000 du Sud de la Mauritanie. Volume 1 géologie. DMG, Ministère des Mines et de l'Industrie.
- Potrel, A., Peucat, J.J., Fanning, C.M., 1998. Archean crustal evolution of the West African Craton: example of the Amsaga Area (Reguibat Rise). U-Pb and Sm-Nd evidence for crustal growth and recycling. Precambrian Res. 90, 107–117. https:// doi.org/10.1016/S0301-9268(98)00044-8.
- Robert, B., Domeier, M., Jakob, J., 2021. On the origins of the Iapetus Ocean. Earth. Sci. Rev. 221, 103791. https://doi.org/10.1016/j.earscirev.2021.103791.
- Rocci, G., Bronner, G., Deschamps, M., 1991. Crystalline Basement of the West African Craton, in: The West African Orogens and Circum-Atlantic Correlatives. Springer Berlin Heidelberg, Berlin, Heidelberg, pp. 31–61. doi: 10.1007/978-3-642-84153-8_ 3.

- Schofield, D.I., Horstwood, M.S.A., Pitfield, P.E.J., Crowley, Q.G., Wilkinson, A.F., Sidaty, H.C.O., 2006. Timing and kinematics of Eburnean tectonics in the central Reguibat Shield. Mauritania. J. Geol. Soc. London. 163, 549–560. https://doi.org/ 10.1144/0016-764905-097.
- Sharman, G.R., Malkowski, M.A., 2020. Needles in a haystack: Detrital zircon U Pb ages and the maximum depositional age of modern global sediment. Earth. Sci. Rev. 203, 103109. https://doi.org/10.1016/j.earscirev.2020.103109.
- Sláma, J., Košler, J., Condon, D.J., Crowley, J.L., Gerdes, A., Hanchar, J.M., Horstwood, M.S.A., Morris, G.A., Nasdala, L., Norberg, N., Schaltegger, U., Schoene, B., Tubrett, M.N., Whitehouse, M.J., 2008. Plešovice zircon — A new natural reference material for U-Pb and Hf isotopic microanalysis. Chem. Geol. 249, 1–35. https://doi.org/10.1016/j.chemgeo.2007.11.005.
- Spencer, C.J., Kirkland, C.L., Taylor, R.J.M., 2016. Strategies towards statistically robust interpretations of in situ U-Pb zircon geochronology. Geosci. Front. 7, 581–589. https://doi.org/10.1016/j.gsf.2015.11.006.
- Stern, R.A., Bodorkos, S., Kamo, S.L., Hickman, A.H., Corfu, F., 2009. Measurement of SIMS Instrumental Mass Fractionation of Pb Isotopes During Zircon Dating. Geostand. Geoanal. Res. 33, 145–168. https://doi.org/10.1111/j.1751-9082-2009-00023 x
- Tohver, E., Trindade, R.I.F., Solum, J.G., Hall, C.M., Riccomini, C., Nogueira, A.C., 2010. Closing the Clymene ocean and bending a Brasiliano belt: Evidence for the Cambrian formation of Gondwana, southeast Amazon craton. Geology 38, 267–270. https://doi.org/10.1130/G30510.1.
- Turner, C.C., Meert, J.G., Pandit, M.K., Kamenov, G.D., 2014. A detrital zircon U–Pb and Hf isotopic transect across the Son Valley sector of the Vindhyan Basin, India: Implications for basin evolution and paleogeography. Gondwana Res. 26, 348–364. https://doi.org/10.1016/j.gr.2013.07.009.
- Ustaömer, P.A., Ustaömer, T., Gerdes, A., Zulauf, G., 2011. Detrital zircon ages from a Lower Ordovician quartzite of the İstanbul exotic terrane (NW Turkey): evidence for

- Amazonian affinity. Int. J. Earth Sci. 100, 23–41. https://doi.org/10.1007/s00531-009-0498-1.
- Vermeesch, P., 2021. Maximum depositional age estimation revisited. Geosci. Front. 12, 843–850. https://doi.org/10.1016/j.gsf.2020.08.008.
- Vermeesch, P., 2013. Multi-sample comparison of detrital age distributions. Chem. Geol. 341, 140–146. https://doi.org/10.1016/j.chemgeo.2013.01.010.
- Vermeesch, P., 2012. On the visualisation of detrital age distributions. Chem. Geol. 312–313, 190–194. https://doi.org/10.1016/j.chemgeo.2012.04.021.
- Vermeesch, P., 2004. How many grains are needed for a provenance study? Earth Planet. Sci. Lett. 224, 441–451. https://doi.org/10.1016/j.epsl.2004.05.037.
- Villeneuve, M., Bellon, H., Guillou, O., Gärtner, A., Mueller, P.A., Heatherington, A.L., Ndiaye, P.M., Theveniaut, H., Corsini, M., Linnemann, U., El Archi, A., Aghzer, A., Youbi, N., 2025. Evolution of the West African fold belts: Review, new geochronological data, new correlations and new geodynamic hypothesis. J. Afr. Earth Sci. 223, 105484. https://doi.org/10.1016/j.jafrearsci.2024.105484.
- Villeneuve, M., Cornée, J.J., 1994. Structure, evolution and palaeogeography of the West African craton and bordering belts during the Neoproterozoic. Precambrian Res. 69, 307–326. https://doi.org/10.1016/0301-9268(94)90094-9.
- Villeneuve, M., Rossignol, C., 2023. Linking the Neoproterozoic to Early Paleozoic Belts Bordering the West African and Amazonian Cratons: Review and New Hypothesis. Minerals 14, 48. https://doi.org/10.3390/min14010048.
- Waldron, J.W.F., Schofield, D.I., Murphy, J.B., Thomas, C.W., 2014. How was the Iapetus Ocean infected with subduction? Geology 42, 1095–1098. https://doi.org/10.1130/ G36194.1.
- Wiedenbeck, M., Allé, P., Corfu, F., Griffin, W.L., Meier, M., Oberli, F., Von Quadt, A., Roddick, J.C., Spiegel, W., 1995. Three natural zircon standards for U-Th-Pb, Lu-Hf, trace element and REE analyses. Geostand. Newsl. 19, 1–23. https://doi.org/ 10.1111/j.1751-908X.1995.tb00147.x.